Research Square

Preprints are preliminary reports that have not undergone peer review.
They should not be considered conclusive, used to inform clinical practice,
or referenced by the media as validated information.

# A Contribution to Resolving the Core Cusp Problem by the Unified Informational Theory

**Amine CHBIHI MOUKIT**

aminechbihi@yahoo.fr

Independent Researcher

**Research Article**

**Keywords:** Cyclic universe, Informational entropy, Dark matter, Core-Cusp problem, density, Galactic dynamics

**Posted Date:** March 27th, 2026

**DOI:** https://doi.org/10.21203/rs.3.rs-8744593/v1

**License:** This work is licensed under a Creative Commons Attribution 4.0 International License.
Read Full License

**Additional Declarations:** No competing interests reported.

# A Contribution to Resolving the Core Cusp Problem by the Unified Informational Theory

By Amine Chbihi Moukit

*Affiliation: Independent Researcher, Marrakech, Morocco.*

Contact : aminechbihi@yahoo.fr

**Abstract:**

We present the Unified Informational Theory (TURI), positing information as the primordial physical substrate. Starting from a cyclic universe with constant entropy ($\Delta S_{cycle} = 0$), we derive a universal profile of density $\rho(r)=\rho_0 sech^8(r/r_c)$ possessing a structural additivity property by convolution.

This profile structurally solves the "Core-Cusp" problem: the condition $d\rho/dr|_{(r\to 0)} = 0$ generates a flat core consistent with observations [1], unlike the singularities of the ΛCDM model. The convergence of the enclosed mass rigorously reproduces the Keplerian laws ($V \propto \sqrt{(1/R)}$). the parameter P = |T×V_rot×mabs| quantifies the compositional homogeneity of the medium [2].

The application to a few massive galaxies suggests the preservation of the $sech^8$ structure at the baryonic level, paving the way for the universality of this distribution for dark and baryonic matter. Our profile strictly preserves Newtonian gravity ($V^2(R) = G.M(R)/R$) without forced modification, revealing that dark and baryonic matter constitute manifestations of a single fundamental informational substrate.

Keywords: Cyclic universe; Informational entropy; Dark matter; Core-Cusp problem; density; Galactic dynamics.

## 1. Introduction

The Unified Informational Theory (TURI) proposes a fundamental paradigm shift: information, rather than mass-energy or spacetime, constitutes the primordial physical substrate. The cyclic universe is envisioned as a continuous alternation between the Big Bang and the Big Crunch [7], thus between phases of expansion and contraction. Recent observational constraints on dark energy, particularly from DESI BAO data [3], suggest deviations from the standard ΛCDM model, with indications that cosmic acceleration may be slowing down.

TURI is based on the assumption of a cyclic universe with constant entropy ($\Delta S_{cycle} = 0$, inspired by von Neumann's entropy conservation theorem [4]). From this single postulate, we derive a universal density profile of the form $\rho(r) = \rho_0 \, \mathrm{sech}^8(r/r_c)$.

This profile possesses remarkable properties:

1. *Structural additivity :*

   The convolution of several profiles in $\mathrm{sech}^8$ yields a profile in $\mathrm{sech}^8$, a signature of self-similarity.

2. *Core-Cusp Resolution :*

   The function $\mathrm{sech}^8$ imposes a zero derivative at the origin ($d\rho/dr|_{(r\to 0)} = 0$), generating a flat density core consistent with observations, unlike the singularities (cusps) of the standard ΛCDM model [5,6]

3. *Convergence of the total mass*:

   Allows for the rigorous rediscovery of Kepler's laws ($V \propto \sqrt{(1/R)}$)

We introduce the observation parameter $P = |T \times V_rot \times m_{abs}|$ where T denotes the morphological index of the system, $V_{rot}$ the rotational speed at a reference radius, and $m_{abs}$ the

absolute magnitude. This parameter allows us to assess the degree of homogeneity of the composition of the medium being studied.

Applying the profile to the cores of some massive galaxies, where the global profile may seem perturbed, suggests that the $sech^8$ structure is preserved at the level of the baryonic core when it is little perturbed. This observation open the way to the robustness of this universal distribution, which could describe both dark and baryonic matter in galaxies. Thus, TURI offers a unified perspective: what we perceived as two distinct entities could be a single signature of information, the fundamental building block constituting the universe.

All the results presented are obtained in accordance with classical Newtonian dynamics. No modification of the law of gravitation is introduced, and the theoretical rotational speed is entirely determined by the enclosed mass via the standard relation $V^2(R) = G \cdot M(R)/R$. The good agreement observed with this model [11] suggests that a coherent classical description can emerge naturally when the mass distribution is correctly modeled.

Note: Detailed calculations for each galaxy studied are included in separate files, in addition to this main article.

## 2. Derivation of ρ(r)

### 2.1 Fundamental Postulate

TURI's fundamental postulate states that the Universe satisfies a cyclic temporal symmetry over a complete cosmological cycle:

$$\Delta S_{cycle} = 0 \quad (1)$$

and therefore:

$$\Delta S_{cycle} = \oint_{Cycle} dS = 0$$

This can also be written as:

$$\int_{-\infty}^{+\infty} dS = \int_{0}^{+\infty} dS + \int_{-\infty}^{0} dS = 0$$

Hence:

$$\int_{0}^{+\infty} dS = -\int_{-\infty}^{0} dS$$

**2.2 Realization of symmetry**

This condition requires that the entropy created in the positive time direction ($\Delta S(+t) > 0$) is exactly compensated by an anti-entropy confined (not directly measurable) in the conjugate time direction ($\Delta S(-t) < 0$). Locally, this is expressed as:

$$\Delta S(+t) + \Delta S(-t) = 0 \quad \Rightarrow \quad \Delta S(+t) = -\Delta S(-t) \quad (2)$$

This symmetry is achieved via two temporally conjugate informational fields [8,9]:

$$\Phi(x^{\mu}) = \phi_p(x^{\mu}) + \phi_f(x^{\mu}) \quad (3)$$

Where :

- $\phi_p$ represents standard causal propagation (past → future, $\Delta S(+t) > 0$)

- $\phi_f$ represents retrocausality confined in an expanding Universe phase (future → past, $\Delta S(-t) < 0$)

The temporal conjugation impose:

$$\phi_f(t) = \phi_p^*(-t) \quad (4)$$

Remark: This relationship remains verified regardless of the observed phase of the universe observed (expansion or contraction).

The total information density becomes:

$$\rho_\phi(t) = |\phi(t)|^2 = \left|\phi_p(t) + \phi_p^*(-t)\right|^2 \quad (5)$$

**2.3 Information Feedback Term**

The development to the lowest order compatible with system dimensions and symmetries leads to the informational feedback term:

$$\Lambda(\rho_\phi) = \kappa \cdot \frac{\rho_\phi}{\rho_0}, \quad \kappa > 0 \quad (6)$$

2.4 Stationary Solutions

We consider stationary solutions of the form:

$$\psi(r,t) = \phi(r)e^{-iEt/\hbar} \quad (7)$$

The system reduces to the following coupled equations:

Nonlinear Schrödinger equation:

$$-\frac{\hbar^2}{2m}\nabla^2\phi + m\Phi\phi + \beta|\phi|^4\phi = E\phi \quad (8)$$

Poisson equation:

$$\nabla^2\Phi = 4\pi G|\phi|^2 \quad (9)$$

where $\beta = (\alpha\kappa/\rho_0) > 0$, with $\alpha$ dimensionless parameter and $\kappa$ retrocausal coupling coefficient.

2.5 Soliton-Type solution: sech⁴ Ansatz

Methodological approach: the exact analytical solution of this coupled non-linear system being intractable, we proceed by ansatz: we propose a candidate functional form and verify that it satisfies equations (8-9) with excellent approximation.

Inspired by solitonic solutions of Gross-Pitaevskii type equations [10], we propose:

$$\phi(r) = \sqrt{A^2 \cdot \mathrm{sech}^{2B}(r/r_c)} \quad (10)$$

Numerical verification: Substituting of this form into equations (8-9) shows that the residuals (difference between left and right sides) remain less than $10^{-6}$ for all r when the parameters satisfy consistency relations with A ≈ 0.319 and B ≈ 5.20 determined numerically, But we choose B=4 (Appendix A).

The corresponding density is:

$$\rho(r) = |\phi(r)|^2 = \rho_0 \cdot \mathrm{sech}^8(r/r_c) \quad (11)$$

where $\rho_0$ and $r_c$ are state variables of the represented system.

Enclosed mass: The mass inside the radius R is expressed as:

$$M(R) = 4\pi\rho_0 r_c^3 \cdot I(u)$$

with $u = R/r_c$ And :

$$I(u) = \int_0^u x^2 \mathrm{sech}^8(x)dx$$

Interpretation: This density profile, resulting from a single fundamental postulate ($\Delta S_{cycle} = 0$), constitutes a theoretical prediction capable of modeling various physical systems in the universe. Its validity must be confronted with observations.

## 3. Universality of ρ(r)

### 3.1 Structural Additivity Property

We observe that the $\mathrm{sech}^8$ profile possesses a remarkable universality characteristic. Indeed, the convolution of two $\mathrm{sech}^8$ profiles (via power 2 of the Fourier transform) produces a profile that fits extremely well with another $\mathrm{sech}^8$, leaving $r_c$ and the amplitude free (the final amplitude remains close to 1 as expected for a normalized density).

3.2 Numerical Convolution Tests

We tested n-body convolutions (from n = 2 to 10). The results show that the n-tuple convolution fits a $\text{sech}^8(r/r'_c)$ profile with a very low relative error (between 0.12% and 0.19% of the maximum amplitude).

Normalization is verified by the integral of the obtained density, very close to 1 (0.997 to 0.9999), confirming numerical accuracy.

The effective radius $r'_c$ increases with n approximately as :

$r'_c \approx a \cdot r_c \cdot \sqrt{n}$

slightly more than pure √n, due to the specific form of $\text{sech}^8$.

3.3 Detailed Results

Table 1: Stability of the $\text{sech}^8$ Profile under convolution

| n | $r'_c$ | $r'_c/(r_c.\sqrt{n})$ | Error % | Complete |
|---|---|---|---|---|
| 2 | 0.924 | 1.037 | 0.117 | 0.99927 |
| 3 | 1.147 | 1.051 | 0.158 | 0.999826 |
| 4 | 1.333 | 1.058 | 0.176 | 0.999682 |
| 5 | 1.496 | 1.062 | 0.184 | 0.999476 |
| 6 | 1.643 | 1.065 | 0.189 | 0.999196 |
| 7 | 1.778 | 1.067 | 0.191 | 0.998831 |
| 8 | 1.904 | 1.068 | 0.191 | 0.998371 |
| 9 | 2.022 | 1.070 | 0.191 | 0.997805 |
| 10 | 2.133 | 1.07 | 0.190 | 0.997121 |

**3.2 Observations**

1. The error remains stable around 0.19% even for n = 10, without significant increase

2. The $\text{sech}^8$ form is remarkably "stable" under multiple convolutions (at least up to n = 10)

3. For moderate n (4, 5, 6), the fit is even better (< 0.19%)

4. The small deviation of the integral of 1 for large n probably comes from the far tails of $\text{sech}^8$, but does not significantly impact the central adjustment.

### 3.3 Conclusion on universality

In an excellent approximate sense, the convolution of n $\text{sech}^8$ profiles produces a form very close to a $\text{sech}^8$ for n = 2 to 10 (and probably beyond).

This characteristic would theoretical allow modeling a nesting of structures with the same profile as that of the elementary components constutung it. This constitutes a potential signature of fundamental unification: different scales of structure could all be described by the same universal profile.

## 4. Conformity with Kepler's Law

### 4.1 Reminder of the density profile

The density is given by the profile:

$$\rho(r) = \rho_0 \cdot \text{sech}^8(r/r_c)$$

where sech(x) = 1/cosh(x).

4.2 Enclosed mass M(R)

The mass contained within a radius R is:

$$M(R) = 4\pi\rho_0 r_c^3 \int_0^{R/r_c} x^2 \text{sech}^8(x)dx$$

On pose u = $R/r_c$ and:

$$I(u) = \int_0^u x^2 \operatorname{sech}^8(x)\,dx$$

Thus:

$$M(R) = 4\pi\rho_0 r_c^3 \cdot I(u) \quad (12)$$

4.3 Total mass

The total mass of the system corresponds to R → ∞, therefore u → ∞:

$$M_{tot} = 4\pi\rho_0 r_c^3 \cdot I(\infty)$$

The value of the integral at infinity, given by the numerical tables (see calculation sheets for galaxies), is:

$$I(\infty) = 0.064873819$$

**4.2 Hypothesis $r_c$ very small compared to R ($r_c$ << R)**

This condition implies that $u = R/r_c$ is very large ($u >> 1$).

The integration shows that I(u) saturates exponentially fast:

| u | I(u) | I(u)/I(∞) |
|---|---|---|
| 1 | 0.0584738086 | ≈ 0.901 |
| 2 | 0.0648592413 | ≈ 0.99978 |
| 3 | 0.064873806 | ≈ 0.9999998 |
| 4 | 0.064873819 | 1 to $10^{-9}$ (approximate) |

Consequence: As soon as $u \geq 4$, we have $I(u) = I(\infty)$ with a precision better than $10^{-9}$. A fortiori for $u >> 4$ (which is typical when $r_c << R$), we have $I(u) = I(\infty)$, therefore :

$$M(R) = 4\pi\rho_0 r_c^3 \cdot I(u) = 4\pi\rho_0 r_c^3 \cdot I(\infty) = M_{tot} \quad \text{(constante)} \quad (13)$$

The enclosed mass is therefore identical to the total mass for any radius R >> $r_c$.

### 4.3 Circular velocity and Kepler's law

The theoretical circular velocity is given by:

$$V(R) = \sqrt{\frac{G \cdot M(R)}{R}}$$

where G is the gravitational constant.

Since M(R) = M_tot (constant), we obtain:

$$V(R) = \sqrt{\frac{G \cdot M_{tot}}{R}} \propto \frac{1}{\sqrt{R}} \quad (14)$$

This is exactly Kepler's law for a point mass.

### 4.4 Generalization

This reasoning is independent of the nature of the central object (Earth, star, galaxy, black hole...).

The only necessary condition is that the concentration scale $r_c$ is very small compared to the observed distances R ($r_c$ << R).

General property: For any system described by $\rho(r) = \rho_0 \, \mathrm{sech}^8(r/r_c)$ with a concentration radius $r_c$ much small compared to the observed distances R, the enclosed mass M(R) becomes constant. It follows that the velocity follows a $1/\sqrt{R}$ law, i.e., Kepler's law.

This property is ensured by the behavior of the integral I(u), which saturates extremely fast (convergence to within $10^{-9}$ as soon as u = 4). In this regime, the $\mathrm{sech}^8$ profile reproduces the behavior of a compact object whose mass is concentrated in a negligible radius, leading to Keplerian dynamics outside.

## 5. Test of the ρ(r) profile on SPARC data

### 5.1 Calculation Method

The TURI model posits a galaxy density profile of the form:

$\rho(r) = \rho_0.\text{sech}^8(r/r_c)$

with a finite total mass $M_{Tot} = \int_0^{infinity} \rho(r) 4\pi . r^2 . dr$

$M_{Tot} = 4\pi . \rho_0 . \int_0^{infinity} r^2 . \text{sech}^8(\frac{r}{r_c}) . dr$

Let $u = R/r_c$ hence:

$M_{Tot} = 4\pi . \rho_0 . \int_0^{infinity} (r_c . u)^2 . (sech^8(u)) . (r_c . du)$

$M_{Tot} = 4\pi . \rho_0 . r_c^3 . \int_0^{infinity} (u)^2 . (sech^8(u)) . du = 4\pi . \rho_0 . r_c^3 .$ I(infinity)

with I(infinity)=0.0648738184

Thus: $\rho_0 = M_{Tot}/(4\pi . r_c^3 .$ I(infinity))

For a galaxy $G_a$ we consider that its total mass (including dark matter) is enclosed within its observed maximum radius:

$M_{Tot} = V_{obs}^2(R_{max}).R_{max}/G$

Substituting in $\rho_0$, we calculate $\rho_0$ of the studied galaxy.

We define $r_c$ for each galaxy as being equal to $R_{max}$ . In some cases, and in order to obtain acceptable accuracy (>70%), we set $r_c$ equal to a fraction of $R_{max}$.

For each observed R, we define the enclosed mass M(R):

$M(R) = \int_0^R \rho(r) 4\pi . r^2 . dr$

$M(R) = 4\pi . \rho_0 . r_c^3 . \int_0^{R/rc} u^2 . \text{sech}^8(u) . du = 4\pi . . \rho_0 . r_c^3 . I(R/r_c)$

We have produced via IA a table of I(u), with precise calculation of the integral from u=0 to 3 by steps of 0.01. For u=3.1 up to u=10 we used a step of 0.1. For values of u not in the table, we proceed by weighted extrapolation between the two values in the table that bracket this u.

Now we can calculate:

$V_{TURI}(r)=\sqrt{(G.M(r)/r)}$

The theoretical $V_{TURI}(r)$ is compared to $V_{observed}(r)$.

The average error is calculated as the mean absolute value of ($V_{TURI}$ - $V_{obs}$) The accuracy in % is calculated as (100-Average Error).

We also calculate, for each galaxy, the $\chi^2$ **:**

$$\chi^2= \sum_i \quad \left(V_{obs,i} - V_{TURI,i}\right)^2/\sigma_i^2$$

with $\sigma_i$ the uncertainty on $V_{obs}$ of point i. The degrees of freedom $d_f$ is the number of observed points minus the number of fixed parameters. Depending on the case, we have:

1- $r_c= R_{max}$ and $\rho_0$ calculated, then $d_f$ equal the number of observation points

2- $r_c$ adjusted as a percentage of $R_{max}$, $d_f$= number of observation points-1

3- $r_c= R_{max}$ and $\rho_0$ adjusted as a percentage of $\rho_0$ calculated, $d_f$= number of observation points–1

4- $r_c$ adjusted as a percentage of $R_{max}$ and $\rho_0$ adjusted as a percentage of $\rho_0$ calculated, $d_f$= number of observation points – 2

We set $\chi^2_{reduced}= \chi^2/d_f$

To investigate whether there is a correlation between $\chi^2_{reduced}$ and specific characteristics of each galaxy, we will use T, $m_{abs}$ and $V_{obs}$ data from HYPERLEDA. This choice is motivated by the fact that our model will theoretically better represent galaxies with a high contribution of dark matter, assumed to have a density only little perturbed by the baryonic component. Galaxies with a mixed contribution of dark and baryonic matter contribution will be poorly represented by our model, notably due to the high central concentration of baryonic mass and the presence of dark matter elsewhere. It should be noted that we will also test the model on the baryonic core of relatively massive galaxies without a very active central black hole.

**5.2 Application to Sparc Galaxies (Sample of 15 galaxies chosen at random)**

5.2.1 Galaxie DDO154

DDO154 (or NGC4789A) is an irregular dwarf galaxy.

Number of points observed: 12

$r_c=R_{max}=5.92$ Kpc , $p_0=p_{0\text{-theoretical}}*1.151$

df=11

Table 2: Observed and TURI Model Rotational Velocities for DDO154

| R | V_Obs | Incer V_Obs | V_TURI | A=(V_obs-V_TURI)^2 | A/Incer V_Obs^2 |
|---|---|---|---|---|---|
| 0,49 | 13,8 | 1,6 | 9,15 | 21,62 | 8,45 |
| 0,99 | 21,6 | 0,8 | 17,93 | 13,47 | 21,05 |
| 1,48 | 28,9 | 0,7 | 25,71 | 10,18 | 20,78 |
| 1,97 | 34,3 | 0,5 | 32,41 | 3,57 | 14,28 |
| 2,47 | 38,2 | 0,4 | 37,92 | 0,08 | 0,5 |
| 2,96 | 42 | 0,2 | 42,01 | 0 | 0 |
| 3,46 | 44,6 | 0,2 | 44,89 | 0,08 | 2 |
| 3,95 | 46,3 | 0,2 | 46,61 | 0,1 | 2,5 |
| 4,44 | 47,4 | 0,3 | 47,43 | 0 | 0 |
| 4,94 | 48,2 | 0,6 | 47,53 | 0,45 | 1,25 |
| 5,43 | 47,4 | 0,7 | 47,11 | 0,08 | 0,16 |
| 5,92 | 45,5 | 1,3 | 46,34 | 0,71 | 0,42 |

Accuracy= 93,9%

$\chi^2/d_f = 6.49$

Figure 1. Rotation Curve: DDO154

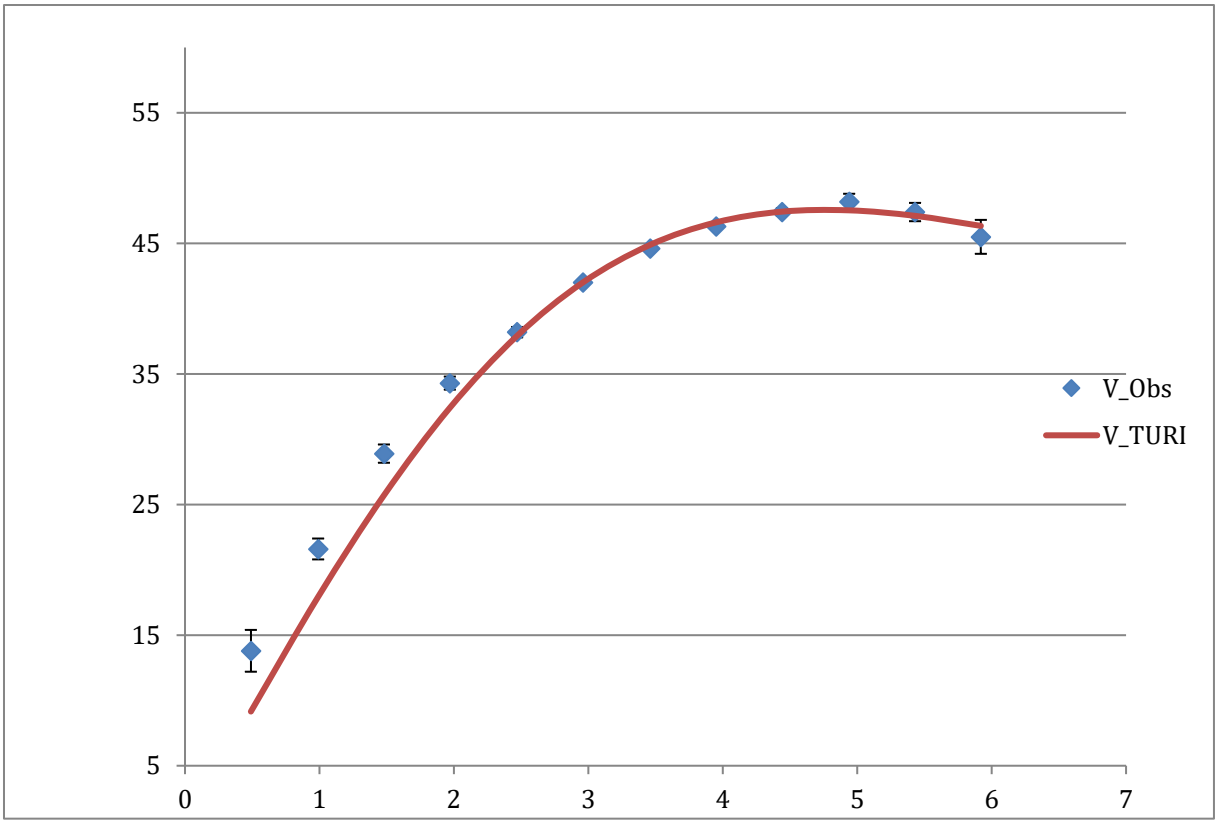



Table 3: HyperLEDA Parameters for DDO154

| HyperLEDA | | | |
|---|---|---|---|
| **T** | **V_rot** | **logr25** | **mabs** |
| 9,9 | 40,1 | 0,18 | -14,3 |

5.2.2 GalaxiesNGC0247

NGC0247 (also known as the Magellanic Needle Galaxy) is an intermediate spiral galaxy of type Scd, characterized by loose spiral arms and a small central nucleus.

Number of points observed: 26

$r_c=R_{max}$ /1.2= 12.117Kpc

p0= $p0_{theor}$ / 1.17 = 22811734.9 Mo/$kpc^3$

df=26-2=24

Table 4: Observed and TURI Model Rotational Velocities for NGC0247

| R | V_Obs | Incer V_Obs | V_TURI | A=(V_obs-V_TURI)^2 | A/Incer V_Obs^2 |
|---|---|---|---|---|---|
| 1,08 | 34,6 | 0,9 | 21,78 | 164,35 | 202,9 |
| 1,61 | 47 | 0,8 | 32,05 | 223,5 | 349,22 |
| 2,15 | 59,1 | 3,1 | 42,05 | 290,7 | 30,25 |
| 2,7 | 64,4 | 1,4 | 51,66 | 162,31 | 82,81 |
| 3,22 | 67,4 | 2,3 | 60,13 | 52,85 | 9,99 |
| 3,77 | 69,8 | 0,7 | 68,32 | 2,19 | 4,47 |
| 4,31 | 71,3 | 1,1 | 75,57 | 18,23 | 15,07 |
| 4,85 | 73,2 | 1,7 | 81,97 | 76,91 | 26,61 |
| 5,38 | 75,1 | 3 | 87,44 | 152,28 | 16,92 |
| 5,92 | 78,5 | 3,8 | 92,17 | 186,87 | 12,94 |
| 6,46 | 81,4 | 5 | 96,09 | 215,8 | 8,63 |
| 6,99 | 83,5 | 7 | 99,19 | 246,18 | 5,02 |
| 7,53 | 87,1 | 7,2 | 101,64 | 211,41 | 4,08 |
| 8,07 | 90,7 | 4,8 | 103,44 | 162,31 | 7,04 |
| 8,62 | 93,1 | 1,4 | 104,67 | 133,86 | 68,3 |
| 9,14 | 95,9 | 2,1 | 105,34 | 89,11 | 20,21 |
| 9,69 | 98,4 | 5,2 | 105,59 | 51,7 | 1,91 |
| 10,23 | 101 | 8,2 | 105,46 | 19,89 | 0,3 |
| 10,76 | 103 | 9,4 | 105,02 | 4,08 | 0,05 |
| 11,3 | 104 | 9,4 | 104,32 | 0,1 | 0 |
| 11,84 | 105 | 8,9 | 103,41 | 2,53 | 0,03 |
| 12,38 | 105 | 8,4 | 102,34 | 7,08 | 0,1 |

| | | | | | |
|---|---|---|---|---|---|
| 12,91 | 105 | 9 | 101,17 | 14,67 | 0,18 |
| 13,48 | 106 | 8,4 | 99,83 | 38,07 | 0,54 |
| 14,01 | 108 | 7,7 | 98,52 | 89,87 | 1,52 |
| 14,54 | 107 | 9,2 | 97,18 | 96,43 | 1,14 |

Accuracy : 87,79%

$\chi^2/d_f = 36,26$

Figure 2. Rotation Curve: NGC0247

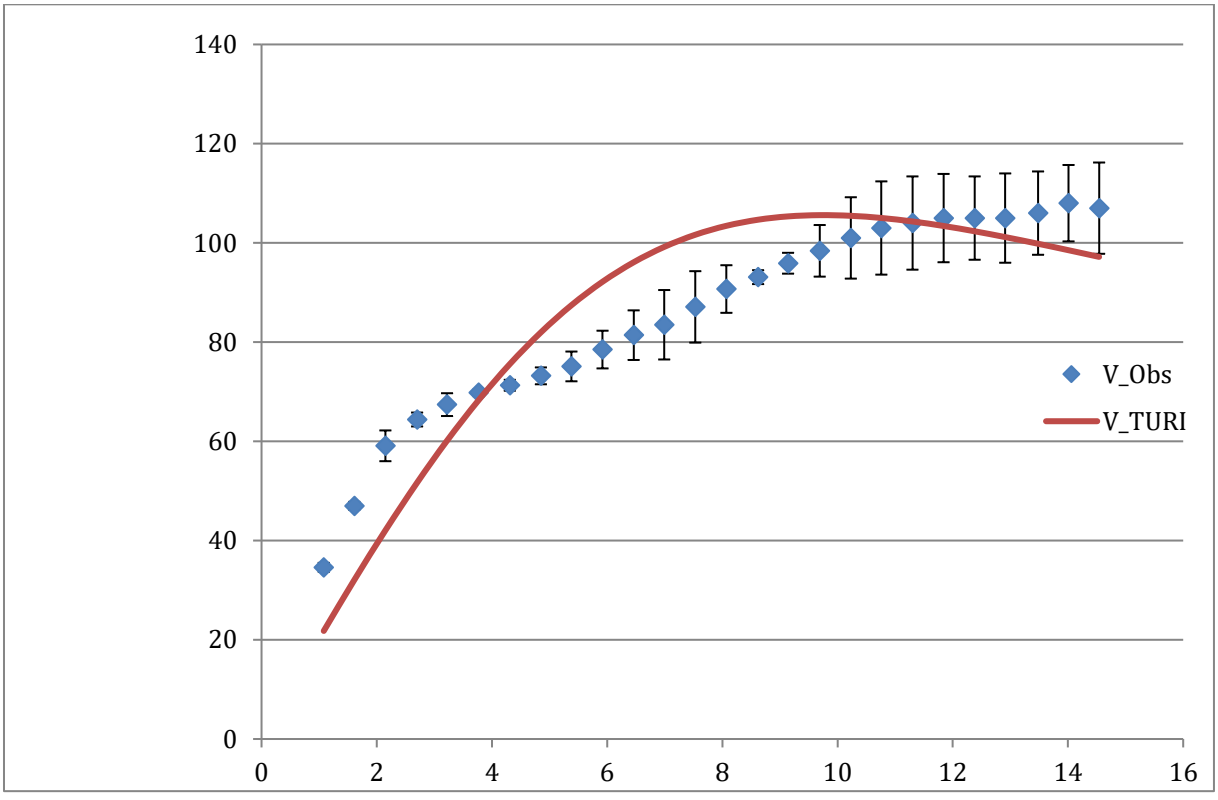



Table 5: HyperLEDA Parameters for NGC0247

| HyperLEDA | | | |
|---|---|---|---|
| **T** | **V_rot** | **logr25** | **mabs** |
| 6,9 | 84,5 | 0,55 | -19,24 |

5.2.3 GalaxiesUGCA444

UGCA444 is an isolated irregular dwarf galaxy.

Number of points observed: 36

$r_c=R_{max}$ = 2.62 Kpc

df=36

Table 6: Observed and TURI Model Rotational Velocities for UGCA444

| R | V_Obs | Incer V_Obs | V_TURI | A=(V_obs-V_TURI)^2 | A/Incer V_Obs^2 |
|---|---|---|---|---|---|
| 0,12 | 6,48 | 2,6 | 4,0789364 | 5,77 | 0,85 |
| 0,19 | 8,6 | 2,65 | 6,3182131 | 5,21 | 0,74 |
| 0,26 | 10,2 | 3,03 | 8,5433608 | 2,74 | 0,3 |
| 0,33 | 11,7 | 3,55 | 10,767456 | 0,87 | 0,07 |
| 0,4 | 12,7 | 3,75 | 12,918114 | 0,05 | 0 |
| 0,47 | 14,1 | 3,43 | 15,003407 | 0,82 | 0,07 |
| 0,55 | 16 | 3,33 | 17,307924 | 1,71 | 0,15 |
| 0,62 | 18,1 | 2,66 | 19,248337 | 1,32 | 0,19 |
| 0,69 | 21,2 | 3,78 | 21,091171 | 0,01 | 0 |
| 0,76 | 21,6 | 3,33 | 22,834959 | 1,53 | 0,14 |
| 0,83 | 23,3 | 3,09 | 24,490065 | 1,42 | 0,15 |
| 0,9 | 24,5 | 3,26 | 26,037514 | 2,36 | 0,22 |
| 0,97 | 24,4 | 3,29 | 27,476977 | 9,47 | 0,87 |
| 1,04 | 25,3 | 2,78 | 28,813854 | 12,35 | 1,6 |
| 1,11 | 25,4 | 2,78 | 30,040796 | 21,54 | 2,79 |
| 1,19 | 25,9 | 2,73 | 31,31131 | 29,28 | 3,93 |
| 1,26 | 26,7 | 2,67 | 32,308896 | 31,46 | 4,41 |
| 1,33 | 27,1 | 3,16 | 33,203175 | 37,25 | 3,73 |

| | | | | | |
|---|---|---|---|---|---|
| 1,4 | 28,6 | 3,34 | 33,99607 | 29,12 | 2,61 |
| 1,48 | 28,9 | 3,21 | 34,782896 | 34,61 | 3,36 |
| 1,55 | 30,4 | 4,14 | 35,371748 | 24,72 | 1,44 |
| 1,62 | 30,8 | 4,35 | 35,871908 | 25,72 | 1,36 |
| 1,69 | 30,5 | 4,56 | 36,288031 | 33,5 | 1,61 |
| 1,75 | 33 | 4,04 | 36,5825 | 12,83 | 0,79 |
| 1,83 | 32,1 | 4,35 | 36,890754 | 22,95 | 1,21 |
| 1,9 | 32,9 | 4,36 | 37,086788 | 17,53 | 0,92 |
| 1,97 | 34,2 | 4,9 | 37,220885 | 9,13 | 0,38 |
| 2,04 | 32,6 | 3,98 | 37,297383 | 22,07 | 1,39 |
| 2,11 | 33,7 | 4,73 | 37,321124 | 13,11 | 0,59 |
| 2,19 | 33,8 | 4,67 | 37,291337 | 12,19 | 0,56 |
| 2,26 | 34,9 | 3,74 | 37,22057 | 5,39 | 0,39 |
| 2,33 | 36,1 | 5,47 | 37,11298 | 1,03 | 0,03 |
| 2,4 | 37,2 | 5,39 | 36,971889 | 0,05 | 0 |
| 2,48 | 37,6 | 7,1 | 36,776462 | 0,68 | 0,01 |
| 2,55 | 35,6 | 4,73 | 36,579275 | 0,96 | 0,04 |
| 2,62 | 38,3 | 7,78 | 36,361746 | 3,76 | 0,06 |

Accuracy: 88.02%

$\chi^2/d_f = 1,03$

Figure 3. Rotation Curve: UGCA444

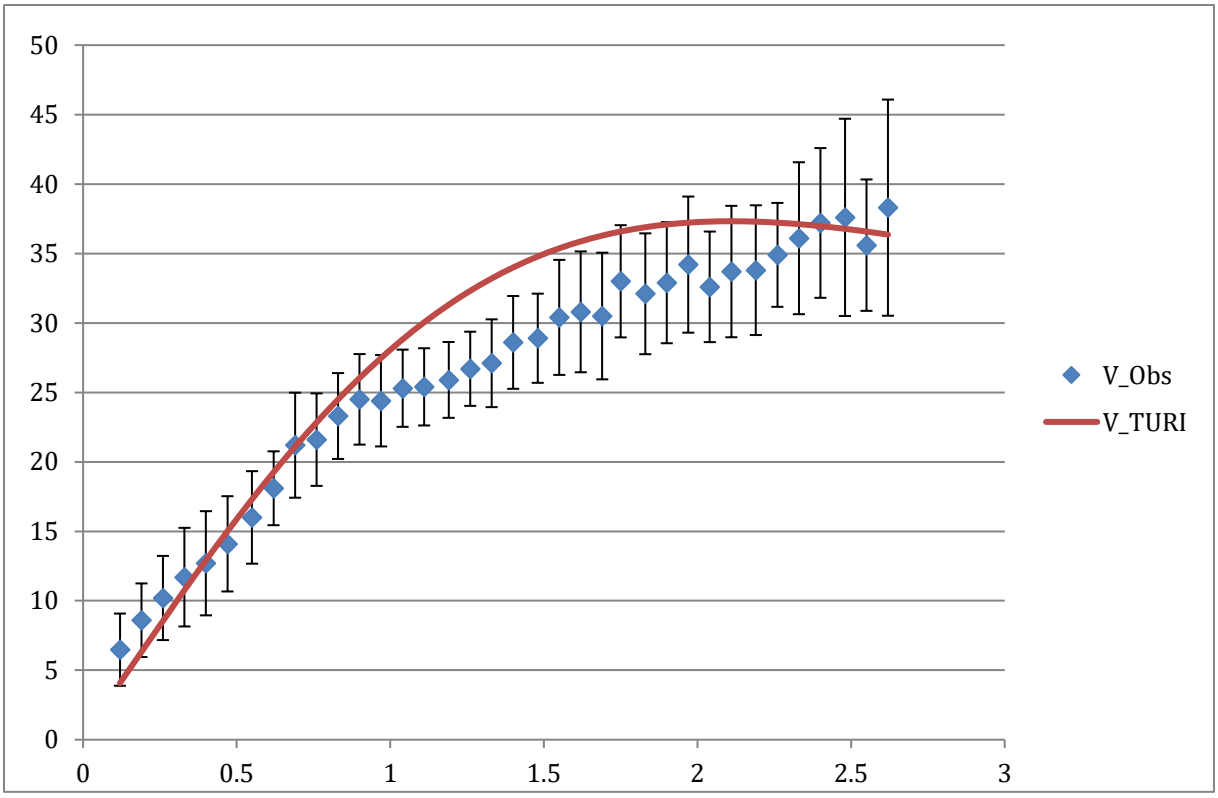



Table 7: HyperLEDA Parameters for UGCA444

| HyperLEDA | | | |
|---|---|---|---|
| **T** | **V_rot** | **logr25** | **mabs** |
| 9,9 | 26,2 | 0,47 | -14,93 |

5.2.4 GalaxiesNGC0289

This is a barred spiral galaxy of type SB(rs)bc. It is characterized by multiple and very extensive spiral arms.

Number of points observed: 28

$r_c=R_{max}/2$ = 35,56 Kpc

df=27

Table 8: Observed and TURI Model Rotational Velocities for NGC0289

| R | V_Obs | Incer V_Obs | V_TURI | A=(V_obs-V_TURI)^2 | A/Incer V_Obs^2 |
|---|---|---|---|---|---|
| 1,5 | 164 | 28,2 | 22,9 | 19909,21 | 25,04 |
| 2,52 | 194 | 32 | 37,53 | 24482,86 | 23,91 |
| 3,46 | 175 | 25,2 | 51,16 | 15336,35 | 24,15 |
| 4,32 | 185 | 31,5 | 63,31 | 14808,46 | 14,92 |
| 5,43 | 175 | 27,9 | 78,72 | 9269,84 | 11,91 |
| 6,38 | 167 | 27,2 | 91,42 | 5712,34 | 7,72 |
| 7,57 | 176 | 7,18 | 106,83 | 4784,49 | 92,81 |
| 10,6 | 185 | 4,29 | 142,22 | 1830,13 | 99,44 |
| 13,57 | 183 | 4,22 | 170,96 | 144,96 | 8,14 |
| 16,64 | 172 | 4,33 | 193,97 | 482,68 | 25,74 |
| 19,71 | 161 | 4,24 | 210,34 | 2434,44 | 135,42 |
| 22,68 | 156 | 5,08 | 220,45 | 4153,8 | 160,96 |
| 25,75 | 159 | 6,49 | 225,91 | 4476,95 | 106,29 |
| 28,72 | 173 | 6,97 | 227,38 | 2957,18 | 60,87 |
| 31,79 | 177 | 6,57 | 225,97 | 2398,06 | 55,56 |
| 34,77 | 179 | 4,47 | 222,65 | 1905,32 | 95,36 |
| 37,84 | 181 | 4,26 | 217,94 | 1364,56 | 75,19 |
| 40,81 | 182 | 4,26 | 212,71 | 943,1 | 51,97 |
| 43,88 | 182 | 4,83 | 207,01 | 625,5 | 26,81 |
| 46,85 | 180 | 5,5 | 201,47 | 460,96 | 15,24 |
| 49,92 | 177 | 8,5 | 195,88 | 356,45 | 4,93 |
| 52,99 | 175 | 11 | 190,55 | 241,8 | 2 |

| | | | | | |
|---|---|---|---|---|---|
| 55,96 | 172 | 11,6 | 185,66 | 186,6 | 1,39 |
| 59,03 | 168 | 12,6 | 180,91 | 166,67 | 1,05 |
| 62 | 158 | 5,38 | 176,61 | 346,33 | 11,97 |
| 65,07 | 158 | 6,5 | 172,44 | 208,51 | 4,94 |
| 68,05 | 166 | 15,5 | 168,65 | 7,02 | 0,03 |
| 71,12 | 165 | 8,75 | 164,98 | 0 | 0 |

Accuracy : 71,3 %

$\chi^2/d_f = 43,99$

Figure 4. Rotation Curve: NGC0289

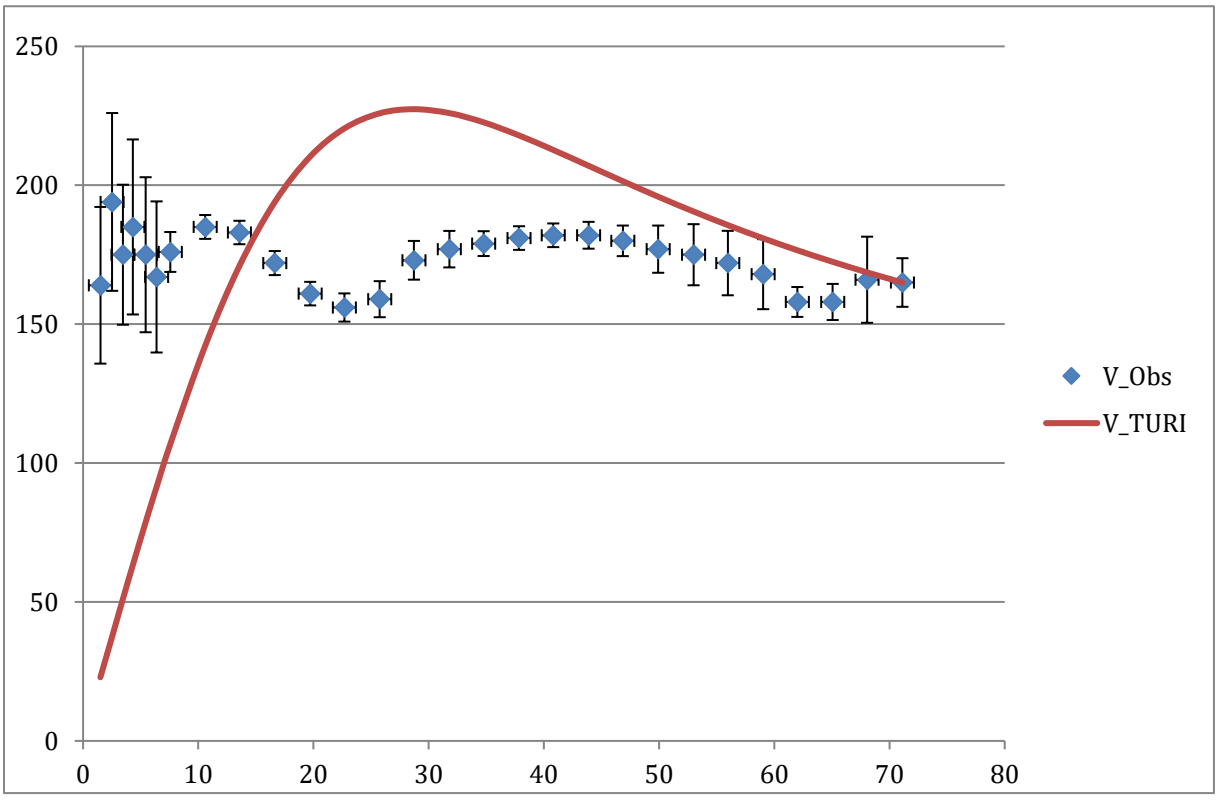



Table 9: HyperLEDA Parameters for NGC0289

| HyperLEDA | | | |
|---|---|---|---|
| **T** | **V_rot** | **logr25** | **mabs** |

| | | | |
|---|---|---|---|
| 4 | 184 | 0,13 | -20,2 |

5.2.5 GalaxiesUGCA442

UGCA442 is a dwarf spiral or irregular galaxy, it is classified as Sd or Sdm.

Number of points observed: 8

$r_c=R_{max}$ = 6,33Kpc

df=8

Table 10: Observed and TURI Model Rotational Velocities for UGCA442

| R | V_Obs | Incer V_Obs | V_TURI | A=(V_obs-V_TURI)^2 | A/Incer V_Obs^2 |
|---|---|---|---|---|---|
| 0,42 | 14,2 | 1,91 | 8,5633121 | 31,77 | 8,71 |
| 1,26 | 28,6 | 1,82 | 24,343356 | 18,12 | 5,47 |
| 2,11 | 41 | 1,74 | 37,558913 | 11,84 | 3,91 |
| 2,96 | 49 | 1,91 | 46,948696 | 4,21 | 1,15 |
| 3,79 | 54,8 | 2,05 | 52,389841 | 5,81 | 1,38 |
| 4,65 | 56,4 | 3,12 | 54,789897 | 2,59 | 0,27 |
| 5,48 | 57,8 | 2,83 | 54,891474 | 8,46 | 1,06 |
| 6,33 | 56,5 | 0,65 | 53,640697 | 8,18 | 19,36 |

Accuracy : 89,44 %

$\chi^2/d_f = 5,16$

Figure 5. Rotation Curve: UGCA442

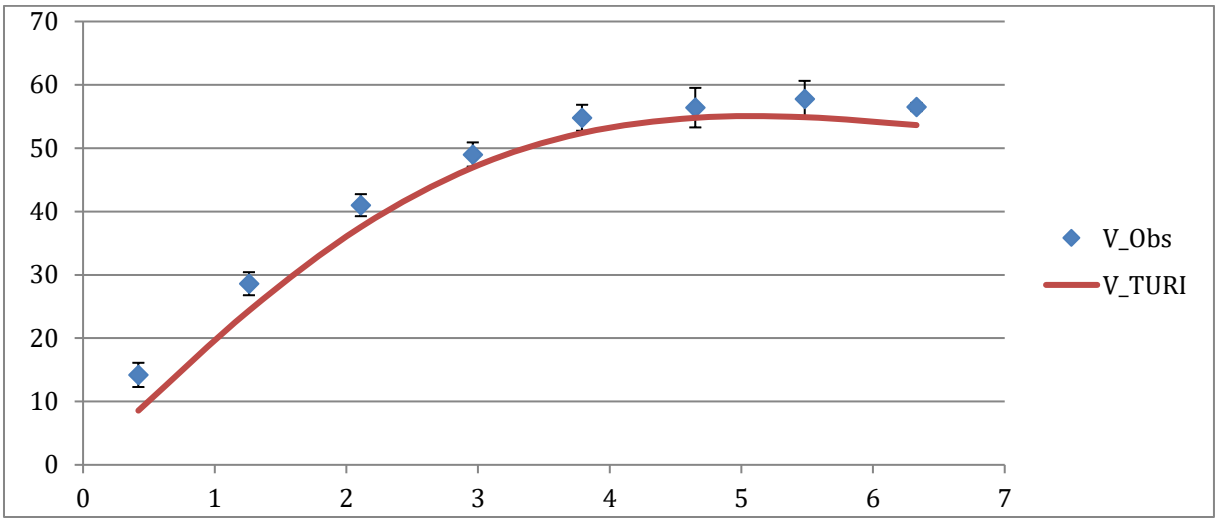



Table 11: HyperLEDA Parameters for UGCA442

| HyperLEDA | | | |
|---|---|---|---|
| **T** | **V_rot** | **logr25** | **mabs** |
| 8,6 | 38,2 | 0,74 | -16,02 |

5.2.6 Galaxy NGC0300

NGC0300 (or Cadwel 70) is a pure spiral galaxy classified as SA(s)d.

Number of points observed: 25

$r_c=R_{max}$ = 11.8Kpc

df=25

Table 12: Observed and TURI Model Rotational Velocities for NGC0300

| R | V_Obs | Incer V_Obs | V_TURI | A=(V_obs-V_TURI)^2 | A/Incer V_Obs^2 |
|---|---|---|---|---|---|
| 0,91 | 33,1 | 3,9 | 16,37 | 279,89 | 18,4 |

| | | | | | |
|---|---|---|---|---|---|
| 1,36 | 46,7 | 2,7 | 24,15 | 508,5 | 69,75 |
| 1,82 | 53,9 | 4,7 | 31,85 | 486,2 | 22,01 |
| 2,27 | 58,8 | 2,5 | 39,07 | 389,27 | 62,28 |
| 2,72 | 65,6 | 2,6 | 45,91 | 387,7 | 57,35 |
| 3,17 | 70,8 | 2,7 | 52,34 | 340,77 | 46,74 |
| 3,63 | 82,1 | 4,9 | 58,43 | 560,27 | 23,33 |
| 4,08 | 84,1 | 6,6 | 63,87 | 409,25 | 9,4 |
| 4,54 | 83,4 | 6,2 | 68,89 | 210,54 | 5,48 |
| 4,99 | 81,5 | 2,7 | 73,25 | 68,06 | 9,34 |
| 5,45 | 80,8 | 4 | 77,16 | 13,25 | 0,83 |
| 5,9 | 82,8 | 12,4 | 80,46 | 5,48 | 0,04 |
| 6,36 | 88,2 | 11,7 | 83,3 | 24,01 | 0,18 |
| 6,81 | 88,5 | 8,5 | 85,6 | 8,41 | 0,12 |
| 7,26 | 88,4 | 8,9 | 87,44 | 0,92 | 0,01 |
| 7,71 | 88,2 | 10,8 | 88,87 | 0,45 | 0 |
| 8,17 | 89,5 | 3,1 | 89,93 | 0,18 | 0,02 |
| 8,62 | 89,7 | 9,5 | 90,62 | 0,85 | 0,01 |
| 9,07 | 93,7 | 7,3 | 91 | 7,29 | 0,14 |
| 9,53 | 97 | 5,7 | 91,11 | 34,69 | 1,07 |
| 9,96 | 96,2 | 1,5 | 90,99 | 27,14 | 12,06 |
| 10,45 | 94,8 | 2,1 | 90,64 | 17,31 | 3,93 |
| 10,93 | 92,5 | 13,9 | 90,11 | 5,71 | 0,03 |
| 11,32 | 92,8 | 10,6 | 89,56 | 10,5 | 0,09 |
| 11,8 | 93,5 | 12,1 | 88,77 | 22,37 | 0,15 |

326

Accuracy : 85.63 %

$\chi^2/d_f = 13.71$

Figure 6. Rotation Curve: NGC0300

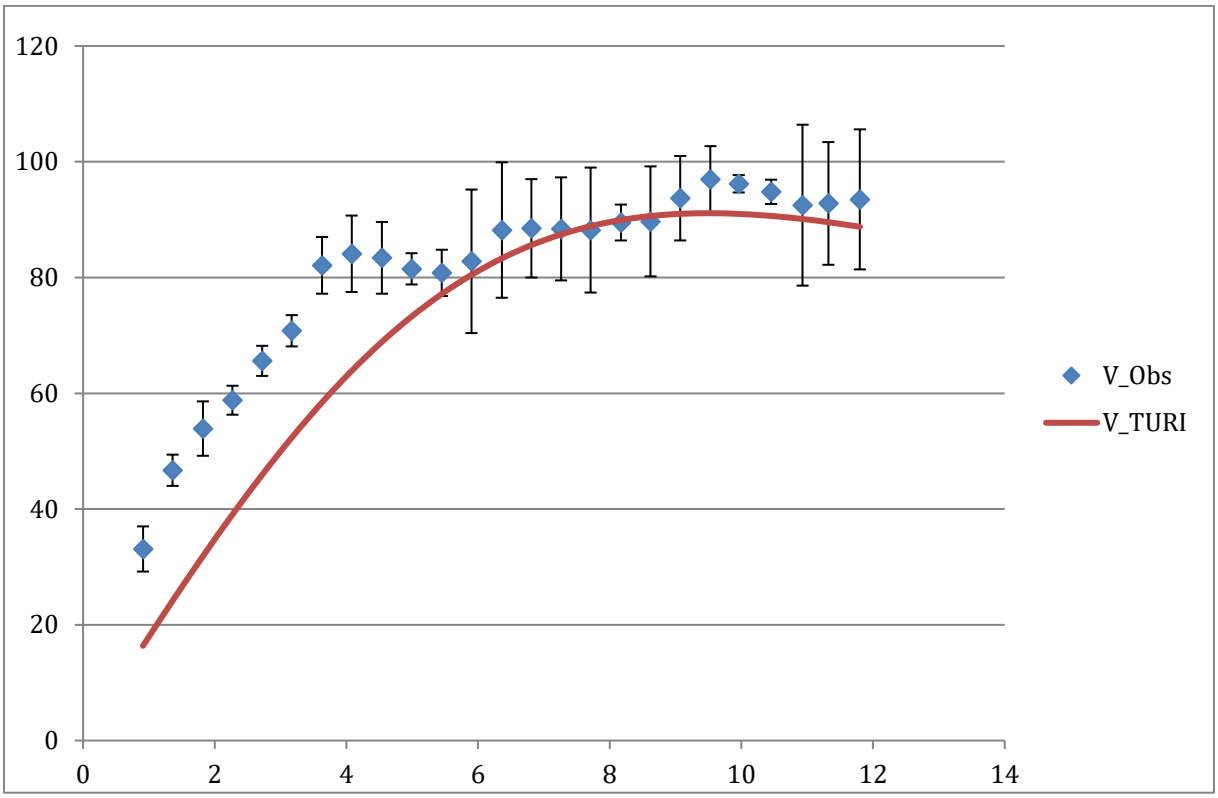



Table 13: HyperLEDA Parameters for NGC0300

| HyperLEDA | | | |
|---|---|---|---|
| **T** | **V_rot** | **logr25** | **mabs** |
| 6,9 | 89,4 | 0,17 | -18,13 |

5.2.7 Galaxy NGC2366

NGC2366 is an irregular dwarf galaxy of type IB(s)m.

Number of points observed: 26

$r_c=R_{max} =$ 6.06Kpc

df=26

Table 14: Observed and TURI Model Rotational Velocities for NGC2366

| R | V_Obs | Incer V_Obs | V_TURI | A=(V_obs-V_TURI)^2 | A/Incer V_Obs^2 |
|---|---|---|---|---|---|
| 0,12 | 4,2 | 3,15 | 2,37 | 3,35 | 0,34 |
| 0,36 | 9,41 | 1,83 | 6,68 | 7,45 | 2,22 |
| 0,59 | 15,3 | 1,37 | 10,84 | 19,89 | 10,6 |
| 0,83 | 18,4 | 1,64 | 15,04 | 11,29 | 4,2 |
| 1,07 | 23,4 | 2,08 | 19,08 | 18,66 | 4,31 |
| 1,31 | 28,1 | 2,46 | 22,93 | 26,73 | 4,42 |
| 1,54 | 33,1 | 2,01 | 26,4 | 44,89 | 11,11 |
| 1,79 | 37,5 | 1,62 | 29,89 | 57,91 | 22,07 |
| 2,02 | 40,5 | 1,68 | 32,84 | 58,68 | 20,79 |
| 2,26 | 42,3 | 1,69 | 35,62 | 44,62 | 15,62 |
| 2,49 | 45,2 | 1,91 | 38,01 | 51,7 | 14,17 |
| 2,74 | 47,4 | 1,95 | 40,28 | 50,69 | 13,33 |
| 2,97 | 48,1 | 1,74 | 42,08 | 36,24 | 11,97 |
| 3,21 | 48,8 | 1,08 | 43,68 | 26,21 | 22,47 |
| 3,44 | 50,7 | 1,55 | 44,95 | 33,06 | 13,76 |
| 3,69 | 52,1 | 2,78 | 46,05 | 36,6 | 4,74 |
| 3,92 | 53 | 2,98 | 46,84 | 37,95 | 4,27 |
| 4,16 | 53,7 | 2,39 | 47,44 | 39,19 | 6,86 |
| 4,4 | 51,2 | 2,21 | 47,84 | 11,29 | 2,31 |
| 4,64 | 51,6 | 1,45 | 48,07 | 12,46 | 5,93 |
| 4,87 | 51,5 | 1,84 | 48,14 | 11,29 | 3,33 |
| 5,11 | 50,4 | 2,53 | 48,08 | 5,38 | 0,84 |

| | | | | | |
|---|---|---|---|---|---|
| 5,35 | 48,5 | 4,6 | 47,91 | 0,35 | 0,02 |
| 5,59 | 50 | 5,91 | 47,64 | 5,57 | 0,16 |
| 5,82 | 49 | 7,42 | 47,31 | 2,86 | 0,05 |
| 6,06 | 49,4 | 5,92 | 46,9 | 6,25 | 0,18 |

Accuracy: 85.72%

$\chi^2/d_f = 7.7$

Figure 7. Rotation Curve: NGC2366

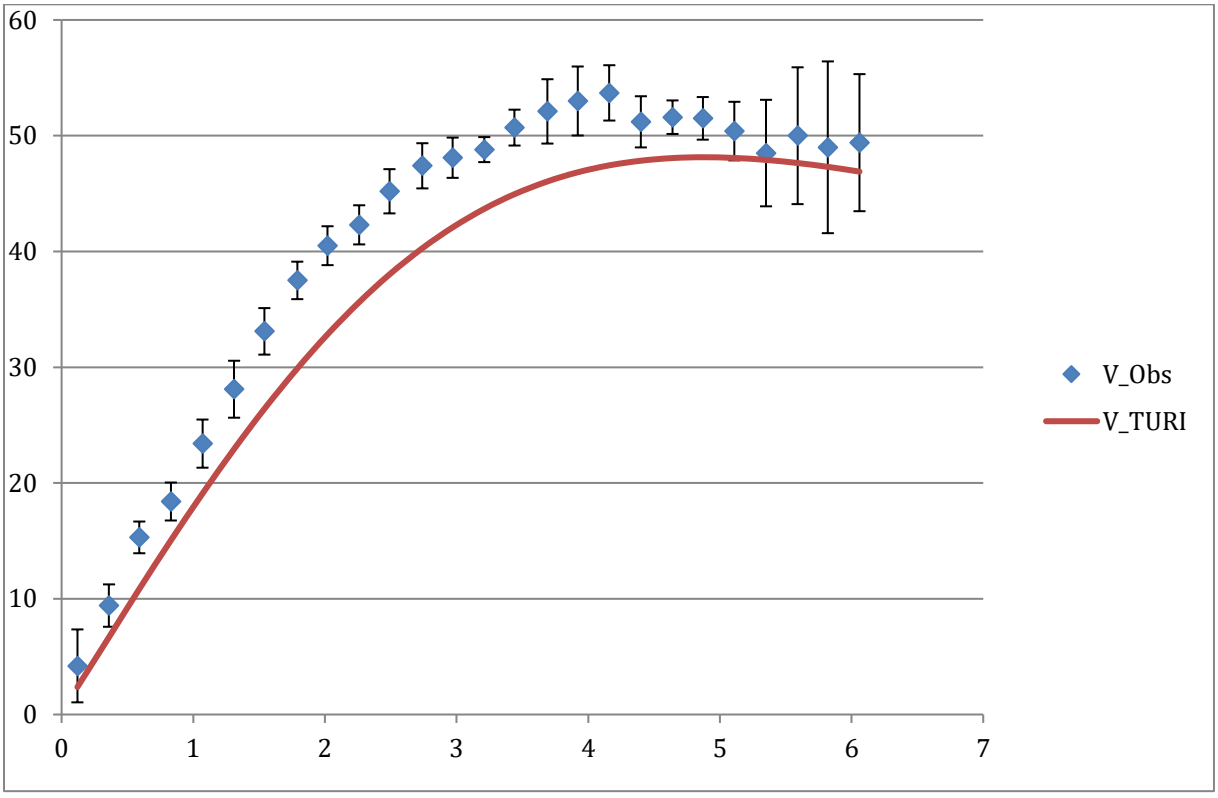



Table 15: HyperLEDA Parameters for NGC2366

| HyperLEDA | | | |
|---|---|---|---|
| **T** | **V_rot** | **logr25** | **mabs** |
| 9,8 | 38,5 | 0,48 | -17,06 |

5.2.8 Galaxie UGC02455

UGC02455 is a barred spiral galaxy classified as SB(s)dm

Number of points observed: 8

$r_c = R_{max} * 1.45 =$ 5,8435Kpc

df=7

Table 16: Observed and TURI Model Rotational Velocities for UGC02455

| R | V_Obs | Incer V_Obs | V_TURI | A=(V_obs-V_TURI)^2 | A/Incer V_Obs^2 |
|---|---|---|---|---|---|
| 0,5 | 16,9 | 3,64 | 9,82 | 50,13 | 3,78 |
| 1 | 23,9 | 3,64 | 19 | 24,01 | 1,81 |
| 1,51 | 28,2 | 3,64 | 27,45 | 0,56 | 0,04 |
| 2,01 | 33 | 3,64 | 34,47 | 2,16 | 0,16 |
| 2,52 | 39,1 | 3,64 | 40,17 | 1,14 | 0,09 |
| 3,02 | 43,8 | 3,64 | 44,29 | 0,24 | 0,02 |
| 3,52 | 53,1 | 3,64 | 47,07 | 36,36 | 2,74 |
| 4,03 | 61 | 3,64 | 48,69 | 151,54 | 11,44 |

Accuracy: 86.88%

$\chi^2/d_f = 2.87$

Figure 8. Rotation Curve: UGC02455

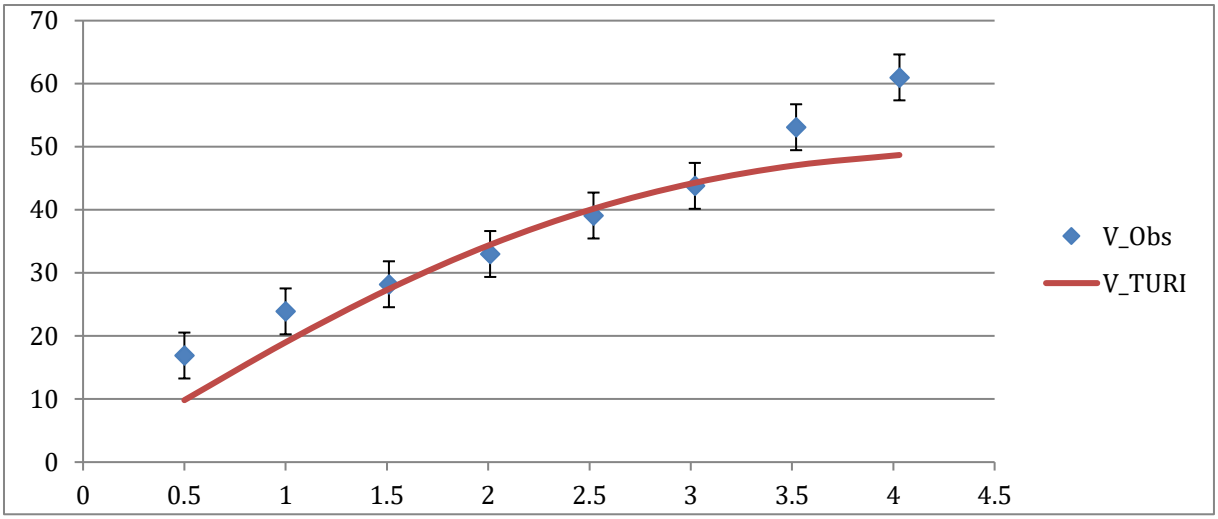



Table 17: HyperLEDA Parameters for UGC02455

| HyperLEDA | | | |
|---|---|---|---|
| **T** | **V_rot** | **logr25** | **mabs** |
| 9,8 | 46,3 | 0,1 | -18,56 |

5.2.9 Galaxy UGC02885

UGC02885 (or Rubin galaxy) is a giant spiral galaxy classified as SA(rs)c.

Number of points observed: 19

$r_c=R_{max}/1.35 =$ 54,867Kpc

df=18

Table 18: Observed and TURI Model Rotational Velocities for UGC02885

| R | V_Obs | Incer V_Obs | V_TURI | A=(V_obs-V_TURI)^2 | A/Incer V_Obs^2 |
|---|---|---|---|---|---|
| 1,7 | 305 | 10 | 25,26 | 78254,47 | 782,54 |
| 3,41 | 257 | 10 | 49,18 | 43189,15 | 431,89 |
| 6,82 | 256 | 10 | 96,13 | 25558,42 | 255,58 |
| 13,67 | 271 | 10 | 181,87 | 7944,16 | 79,44 |

| | | | | | |
|---|---|---|---|---|---|
| 19,49 | 282 | 10 | 241,22 | 1663,01 | 16,63 |
| 23,36 | 287 | 10 | 272,41 | 212,87 | 2,13 |
| 27,24 | 283 | 10 | 296,91 | 193,49 | 1,93 |
| 31,22 | 280 | 10 | 315,33 | 1248,21 | 12,48 |
| 35,1 | 280 | 10 | 327,37 | 2243,92 | 22,44 |
| 38,97 | 281 | 10 | 334,36 | 2847,29 | 28,47 |
| 42,85 | 282 | 10 | 337,22 | 3049,25 | 30,49 |
| 46,73 | 287 | 10 | 336,79 | 2479,04 | 24,79 |
| 50,71 | 292 | 10 | 333,79 | 1746,4 | 17,46 |
| 54,58 | 298 | 10 | 329,12 | 968,45 | 9,68 |
| 58,46 | 298 | 10 | 323,27 | 638,57 | 6,39 |
| 62,34 | 298 | 10 | 316,73 | 350,81 | 3,51 |
| 66,21 | 298 | 10 | 309,85 | 140,42 | 1,4 |
| 70,19 | 298 | 10 | 302,69 | 22 | 0,22 |
| 74,07 | 298 | 10 | 295,79 | 4,88 | 0,05 |

Accuracy: 77.7%

$\chi^2/d_f = 95.97$

Figure 9. Rotation Curve: UGC02885

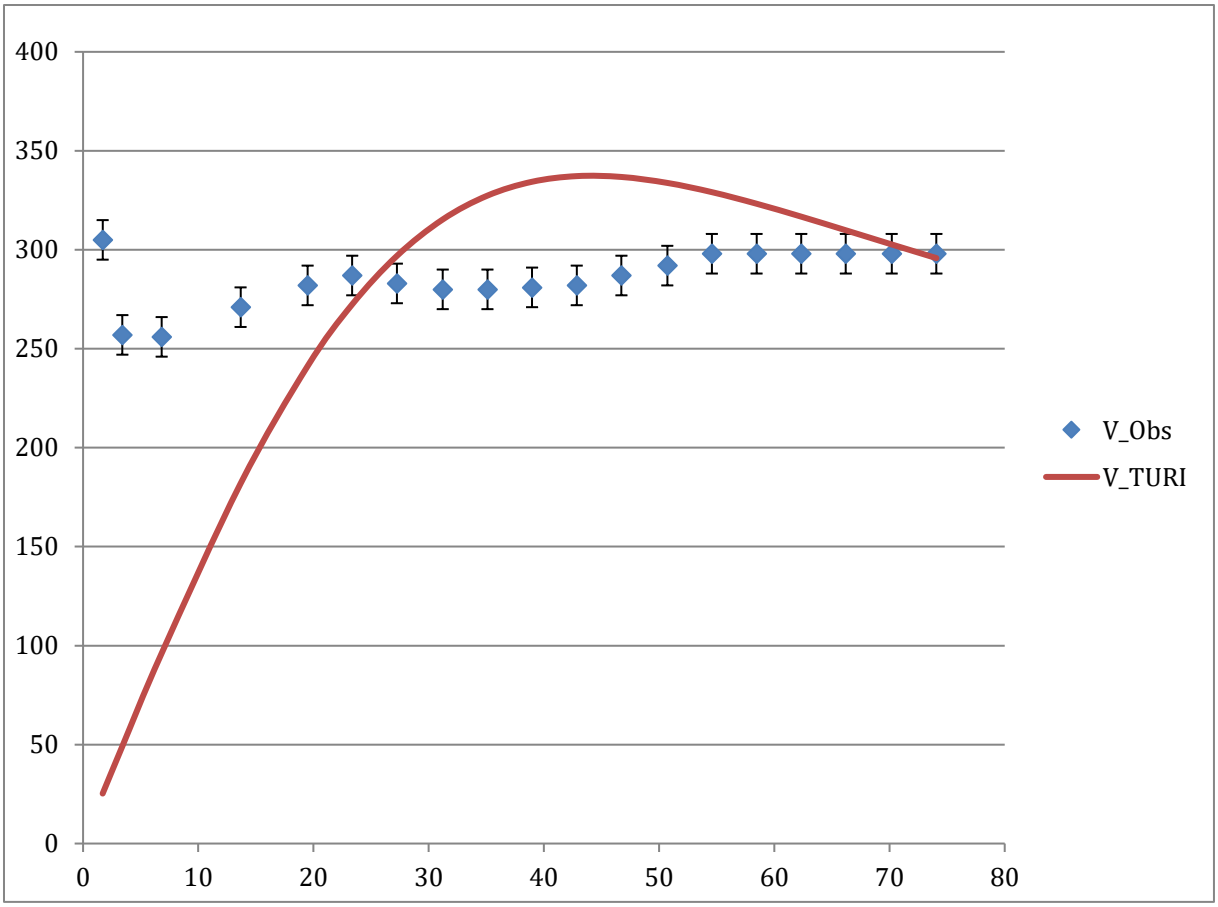



Table 19: HyperLEDA Parameters for UGC02885

| HyperLEDA | | | |
|---|---|---|---|
| **T** | **V_rot** | **logr25** | **mabs** |
| 5,2 | 294,6 | 0,31 | -21,86 |

## 5.2.10 Galaxy UGC06614

UGC06614 is a giant spiral galaxy of type (R)SA(r)ab.

Number of points observed: 13

$r_c=R_{max}/1.82 =$ 35.49Kpc

df=12

Table 20: Observed and TURI Model Rotational Velocities for UGC06614

| R | V_Obs | Incer V_Obs | V_TURI | A=(V_obs-V_TURI)^2 | A/Incer V_Obs^2 |
|---|---|---|---|---|---|
| 3,23 | 194 | 16,7 | 53,7 | 19684,09 | 70,58 |
| 9,18 | 172 | 8,1 | 141,94 | 903,6 | 13,77 |
| 10,64 | 170 | 10,7 | 160,23 | 95,45 | 0,83 |
| 11,58 | 170 | 6,8 | 171,2 | 1,44 | 0,03 |
| 12,52 | 171 | 6,8 | 181,43 | 108,78 | 2,35 |
| 13,57 | 172 | 12,1 | 192,01 | 400,4 | 2,73 |
| 15,76 | 174 | 19,6 | 211,19 | 1383,1 | 3,6 |
| 24,94 | 193 | 23,2 | 252,33 | 3520,05 | 6,54 |
| 26,3 | 194 | 23 | 254,03 | 3603,6 | 6,81 |
| 34,96 | 201 | 7,2 | 249,32 | 2334,82 | 45,04 |
| 36,84 | 202 | 17,1 | 246,15 | 1949,22 | 6,67 |
| 47,38 | 205 | 16 | 224,67 | 386,91 | 1,51 |
| 64,59 | 204 | 16 | 193,93 | 101,4 | 0,4 |

Accuracy: 80.19%

$\chi^2/d_f = 13.41$

Figure 10. Rotation Curve: UGC06614

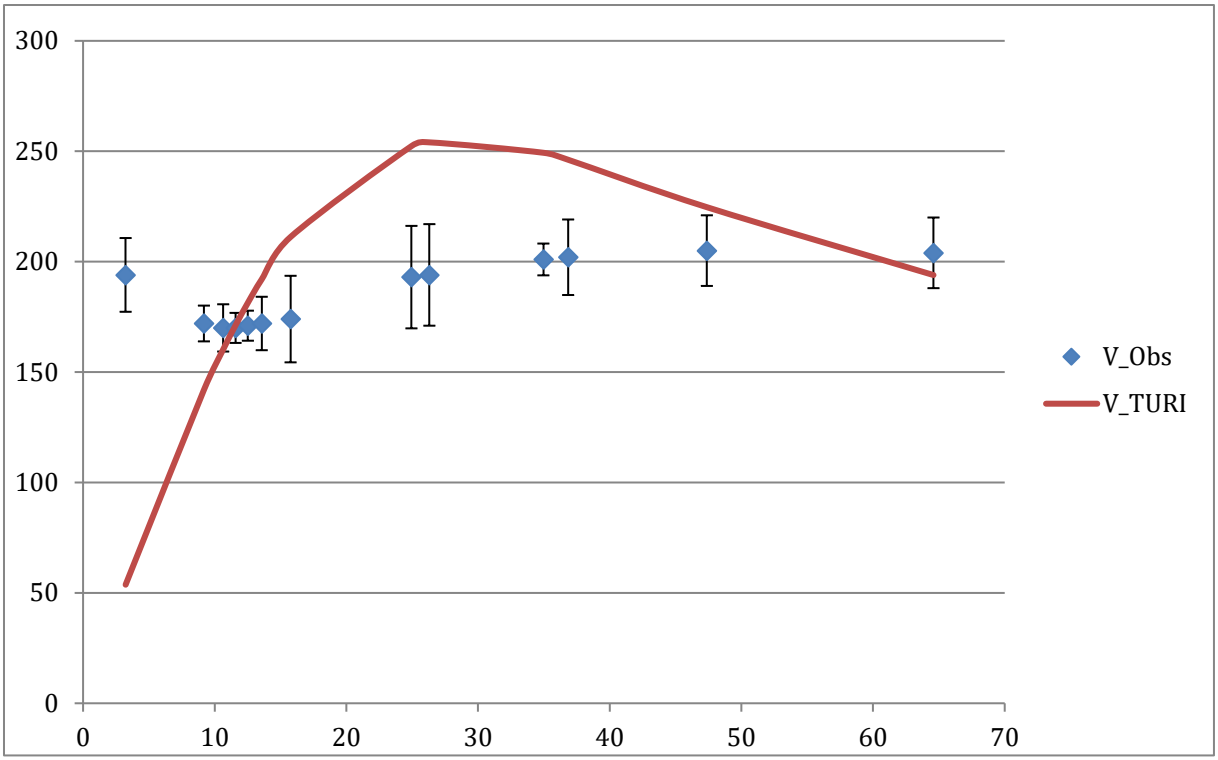



Table 21: HyperLEDA Parameters for UGC06614

| HyperLEDA | | | |
|---|---|---|---|
| **T** | **V_rot** | **logr25** | **mabs** |
| 1 | 231,9 | 0,05 | -20,72 |

5.2.11 Galaxy UGC06628

UGC06628, also listed as PGC36240, is an Sd-type spiral galaxy.

Number of points observed: 7

$r_c=R_{max}$ = 7.69Kpc

df=7

Table 22: Observed and TURI Model Rotational Velocities for UGC06628

| R | V_Obs | Incer V_Obs | V_TURI | A=(V_obs-V_TURI)^2 | A/Incer V_Obs^2 |
|---|---|---|---|---|---|
| 1,1 | 26,9 | 8,27 | 13,42 | 181,71 | 2,66 |

| | | | | | |
|---|---|---|---|---|---|
| 2,2 | 38 | 8,27 | 24,94 | 170,56 | 2,49 |
| 3,3 | 40,5 | 8,27 | 33,44 | 49,84 | 0,73 |
| 4,39 | 41,4 | 8,27 | 38,57 | 8,01 | 0,12 |
| 5,5 | 42,3 | 8,27 | 40,89 | 1,99 | 0,03 |
| 6,59 | 42,3 | 8,27 | 41,13 | 1,37 | 0,02 |
| 7,69 | 42,3 | 8,27 | 40,16 | 4,58 | 0,07 |

Accuracy: 82.87%

$\chi^2/d_f = 0.87$

Figure 11. Rotation Curve: UGC06628

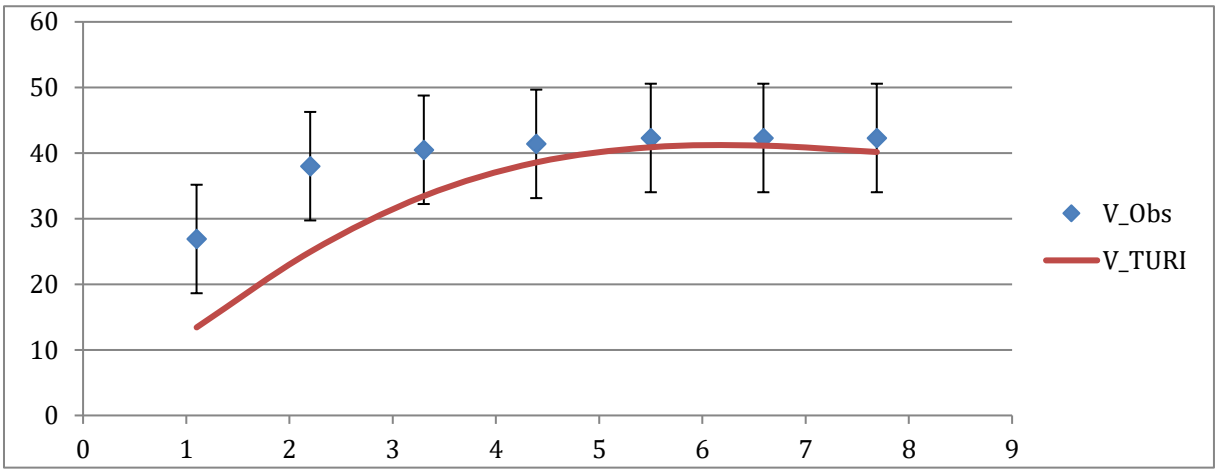



Table 23: HyperLEDA Parameters for UGC06628

| HyperLEDA | | | |
|---|---|---|---|
| **T** | **V_rot** | **logr25** | **mabs** |
| 8.8 | 30 | 0,58 | -17.96 |

5.2.12 Galaxy UGC07232

UGC07232 is a dwarf, or low-mass, barred spiral galaxy classified as SB(s)m.

Number of points observed: 4

401 $r_c=R_{max}*1.2 =$ 0,984Kpc

402 df=3

403 Table 24: Observed and TURI Model Rotational Velocities for UGC07232

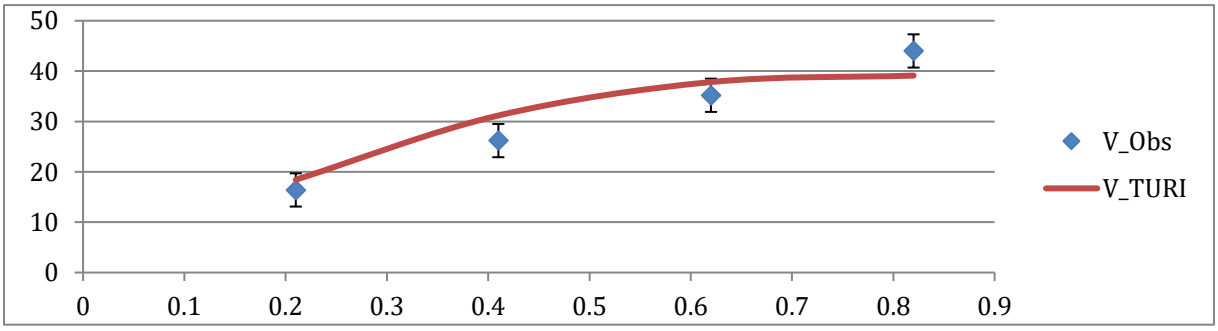
| R | V_Obs | Incer V_Obs | V_TURI | A=(V_obs-V_TURI)^2 | A/Incer V_Obs^2 |
|---|---|---|---|---|---|
| 0,21 | 16,4 | 3,3 | 18,43 | 4,12 | 0,38 |
| 0,41 | 26,2 | 3,3 | 31,18 | 24,8 | 2,28 |
| 0,62 | 35,2 | 3,3 | 37,82 | 6,86 | 0,63 |
| 0,82 | 44 | 3,3 | 39,11 | 23,91 | 2,2 |

404

405 Accuracy: 87.51%

406 $\chi^2/d_f = 1.83$

407 Figure 12. Rotation Curve: UGC07232




408

409 Table 25: HyperLEDA Parameters for UGC07232

| HyperLEDA | | | |
|---|---|---|---|
| **T** | **V_rot** | **logr25** | **mabs** |
| 9,9 | 41,1 | 0,04 | -13,61 |

410

411 5.2.13 Galaxy UGC12732

412 UGC12732 is a spiral galaxy of type Sd or Sm, with a discrete nucleus and irregular spiral arms.

Number of points observed: 16

$r_c=R_{max}$ = 15.4Kpc

df=16

Table 26: Observed and TURI Model Rotational Velocities for UGC12732

| R | V_Obs | Incer V_Obs | V_TURI | A=(V_obs-V_TURI)^2 | A/Incer V_Obs^2 |
|---|---|---|---|---|---|
| 0,96 | 34,2 | 3,32 | 13,96 | 409,66 | 37,17 |
| 1,92 | 49,5 | 4,6 | 27,29 | 493,28 | 23,31 |
| 2,88 | 59,9 | 4,38 | 39,91 | 399,6 | 20,83 |
| 3,84 | 65,3 | 4,31 | 51,51 | 190,16 | 10,24 |
| 4,8 | 69,8 | 3,83 | 61,87 | 62,88 | 4,29 |
| 5,76 | 73,8 | 3,45 | 70,82 | 8,88 | 0,75 |
| 6,72 | 76,2 | 3,24 | 78,26 | 4,24 | 0,4 |
| 7,68 | 79,3 | 3,19 | 84,22 | 24,21 | 2,38 |
| 8,64 | 80,3 | 3,31 | 88,76 | 71,57 | 6,53 |
| 9,6 | 81,9 | 3,69 | 92 | 102,01 | 7,49 |
| 10,6 | 84 | 3,89 | 94,16 | 103,23 | 6,82 |
| 11,5 | 85,6 | 3,67 | 95,18 | 91,78 | 6,81 |
| 12,5 | 87,9 | 3,43 | 95,49 | 57,61 | 4,9 |
| 13,4 | 90,8 | 3,36 | 95,17 | 19,1 | 1,69 |
| 14,4 | 95,5 | 3,18 | 94,3 | 1,44 | 0,14 |
| 15,4 | 98 | 3,18 | 93,04 | 24,6 | 2,43 |

Accuracy: 84.45%

$\chi^2/d_f = 8.51$

Figure 13. Rotation Curve: UGC12732

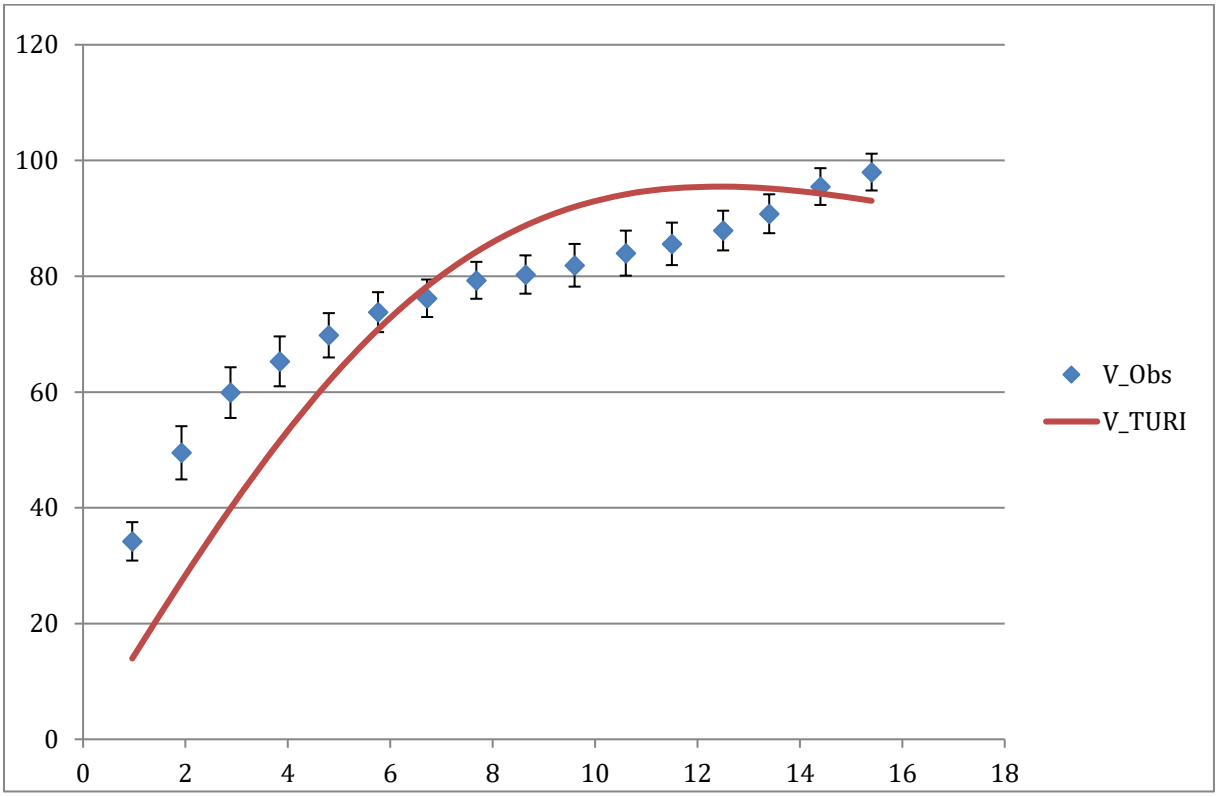



Table 27: HyperLEDA Parameters for UGC12732

| HyperLEDA | | | |
|---|---|---|---|
| **T** | **V_rot** | **logr25** | **mabs** |
| 8,7 | 149,6 | 0,02 | -16,45 |

5.2.14 Galaxy UGCA281

UGCA281 is a blue compact dwarf (BCD) galaxy.

Number of points observed: 7

$r_c=R_{max}$ = 1.08Kpc

df=7

Table 28: Observed and TURI Model Rotational Velocities for UGCA281

| R | V_Obs | Incer V_Obs | V_TURI | A=(V_obs-V_TURI)^2 | A/Incer V_Obs^2 |
|---|---|---|---|---|---|
| 0,09 | 7 | 2,49 | 5,5710514 | 2,041894 | 0,3293324 |
| 0,25 | 14,9 | 1,35 | 14,540821 | 0,1290097 | 0,0707872 |
| 0,41 | 21,1 | 1,37 | 21,535169 | 0,1893723 | 0,1008963 |
| 0,58 | 26 | 1,24 | 26,242176 | 0,0586493 | 0,0381434 |
| 0,74 | 27,5 | 1,59 | 28,31972 | 0,6719407 | 0,2657888 |
| 0,9 | 28,8 | 2,57 | 28,726729 | 0,0053686 | 0,0008128 |
| 1,08 | 29,5 | 1,85 | 28,007089 | 2,2287823 | 0,6512147 |

Accuracy: 95.13%

$\chi^2/d_f = 0.21$

Figure 14. Rotation Curve: UGCA281

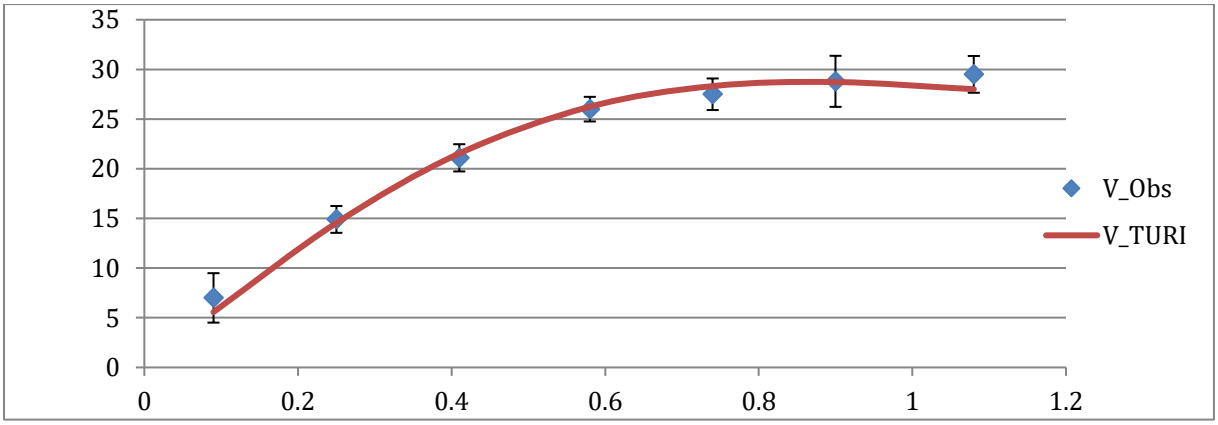



Table 29: HyperLEDA Parameters for UGCA281

| HyperLEDA | | | |
|---|---|---|---|
| **T** | **V_rot** | **logr25** | **mabs** |
| 10 | 26,2 | 0,12 | -14,52 |

5.2.15 Galaxy NGC5005

NGC5005 (or Caldwell 29) is an intermediate spiral galaxy classified as SAB(rs)bc. It exhibits a discrete central bar and multiple spiral arms.

Number of points observed: 18

$r_c=R_{max}/1.5$ = 7,647Kpc

df=17

Table 30: Observed and TURI Model Rotational Velocities for NGC5005

| R | V_Obs | Incer V_Obs | V_TURI | A=(V_obs-V_TURI)^2 | A/Incer V_Obs^2 |
|---|---|---|---|---|---|
| 0,49 | 211 | 40,1 | 47,59 | 26702,83 | 16,61 |
| 0,98 | 233 | 17,4 | 92,7 | 19684,09 | 65,02 |
| 1,47 | 227 | 14,4 | 135,52 | 8368,59 | 40,36 |
| 1,97 | 234 | 10,8 | 175,43 | 3430,44 | 29,41 |
| 2,46 | 245 | 7,67 | 210 | 1225 | 20,82 |
| 2,95 | 244 | 23,3 | 239,56 | 19,71 | 0,04 |
| 3,44 | 261 | 23,3 | 263,87 | 8,24 | 0,02 |
| 3,93 | 259 | 22,7 | 283,03 | 577,44 | 1,12 |
| 4,42 | 258 | 22,7 | 297,3 | 1544,49 | 3 |
| 4,92 | 258 | 22,5 | 307,31 | 2431,48 | 4,8 |
| 5,74 | 261 | 22,4 | 315,37 | 2956,1 | 5,89 |
| 6,56 | 263 | 22,4 | 315,54 | 2760,45 | 5,5 |
| 7,37 | 264 | 22,3 | 310,59 | 2170,63 | 4,36 |
| 8,19 | 265 | 22,2 | 302,56 | 1410,75 | 2,86 |
| 9,01 | 265 | 22,2 | 293,07 | 787,92 | 1,6 |
| 9,83 | 264 | 22 | 283,15 | 366,72 | 0,76 |
| 10,65 | 264 | 21,9 | 273,43 | 88,92 | 0,19 |

| | | | | | |
|---|---|---|---|---|---|
| 11,47 | 265 | 22 | 264,21 | 0,62 | 0 |

Accuracy: 80.1%

$\chi^2/d_f = 11.9$

Figure 15. Rotation Curve: NGC5005

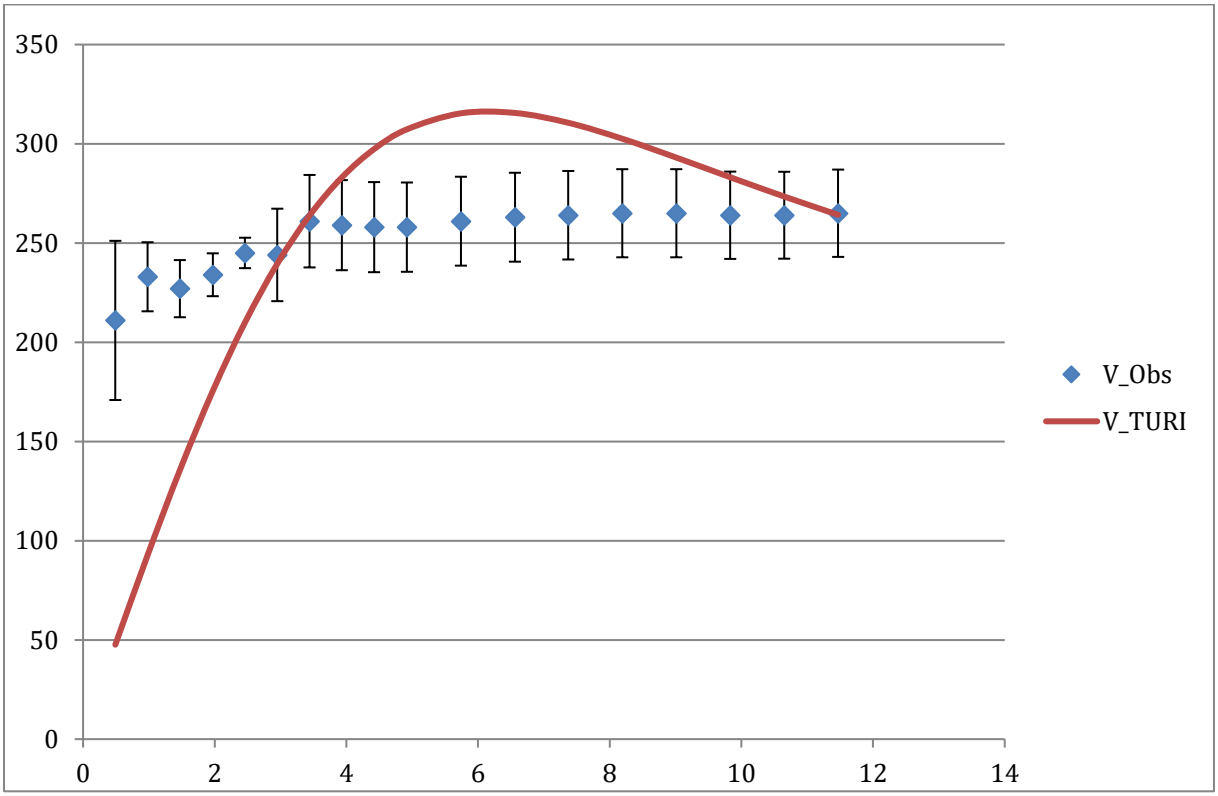



Table 31: HyperLEDA Parameters for NGC5005

| HyperLEDA | | | |
|---|---|---|---|
| **T** | **V_rot** | **logr25** | **mabs** |
| 4 | 251 | 0,5 | -21,96 |

### 5.3 Correlation Coefficient

We sought to find a correlation between $\chi^2/d_f$ of our model and the intrinsic characteristics of galaxies. We found that $\chi^2/d_f$ correlates strongly (r=0.774) with the absolute value of the product $T*V_{rot}*mabs$.

Table 32: Correlation between $\chi 2/df$ and $|T \times Vrot \times mabs|$

| | Calculated | HyperLEDA | | | |
|---|---|---|---|---|---|
| **Designation** | **X^2/df** | **T** | **V_rot** | **mabs** | **abs(T*V_rot*mabs)** |
| DDO154 | 6,49 | 9,9 | 40,1 | -14,3 | 5676,96 |
| NGC0247 | 36,26 | 6,9 | 84,5 | -19,24 | 11217,88 |
| NGC0289 | 43,99 | 4 | 184 | -20,2 | 14867,20 |
| NGC0300 | 13,71 | 6,9 | 89,4 | -18,13 | 11183,67 |
| NGC2366 | 7,7 | 9,8 | 38,5 | -17,06 | 6436,74 |
| NGC5005 | 11,9 | 4 | 251 | -21,96 | 22047,84 |
| UGC02455 | 2,87 | 9,8 | 46,3 | -18,56 | 8421,41 |
| UGC02885 | 95,97 | 5,2 | 294,6 | -21,86 | 33487,77 |
| UGC06614 | 13,41 | 1 | 231,9 | -20,72 | 4804,97 |
| UGC06628 | 0,87 | 8,8 | 30 | -17,96 | 4741,44 |
| UGC07232 | 1,83 | 9,9 | 41,1 | -13,61 | 5537,77 |
| UGC12732 | 8,51 | 8,7 | 149,6 | -16,45 | 21410,00 |
| UGCA281 | 0,21 | 10 | 26,2 | -14,52 | 3804,24 |
| UGCA442 | 5,16 | 8,6 | 38,2 | -16,02 | 5262,89 |
| UGCA444 | 1,03 | 9,9 | 26,2 | -14,93 | 3872,54 |

The objective of what follows is to physically motivate the use of a simple composite parameter, constructed from standard observables, to characterize the dynamic regime of galaxies and their relative degree of baryonic or dark matter dominance. The considered parameter is the absolute value of the product between the morphological index T, the rotational velocity $V_{rot}$ and the absolute magnitude $m_{abs}$.

5.3.1 Basic quantities and physical significance

Morphological index T: The morphological index T describes the global baryonic structure of the galaxy. For spiral galaxies (T greater than zero), an increasing value of T corresponds to a decreasing bulge/disk ratio and a more extended baryonic distribution. For elliptical and lenticular galaxies (T less than or equal to zero), negative values of T indicate a spheroidal morphology dominated by a strong central concentration of baryons. The index T can thus be interpreted as an empirical proxy for the central baryonic concentration.

Rotation velocity $V_{rot}$ : Rotational velocity is a direct measure of the total dynamic mass. At a given radius, it is related to the total mass contained within that radius, including both the baryonic component and dark matter. $V_{rot}$ thus constitutes a global tracer of the depth of the galaxy's gravitational potential.

Absolute magnitude $m_{abs}$ : Absolute magnitude is an indicator of stellar mass. Under the assumption of a reasonable mass-to-luminosity ratio, luminosity increases with stellar mass. More negative $m_{abs}$ values correspond to more luminous and therefore, on average, more massive galaxies from a stellar baryonic perspective.

5.3.2 Construction and motivation of the composite parameter

The composite parameter is defined as the absolute value of the product $P=T\times V_{rot}\times_{mabs}$. This product is not a fundamental quantity, but an empirical combination. Taking the absolute value allows us to characterize the overall amplitude of this combination independently of the sign of T or $m_{abs}$.

This parameter can be heuristically interpreted as a synthetic measure of the joint importance of baryonic concentration, gravitational potential depth, and stellar mass.

At the effective radius scale, the dynamical mass depends on the square of the rotational velocity and the characteristic size of the galaxy. The effective size is itself correlated with luminosity by well-established size-luminosity relations. The baryon ratio, defined as the ratio

between stellar mass and dynamical mass, therefore depends directly on the luminosity, rotational velocity, and the spatial structure of the galaxy.

Although the parameter P is not equivalent to the baryon ratio, it precisely combines observables that control this ratio. It is thus expected to be correlated with the degree of baryon dominance or dark matter dominance in the inner regions of galaxies.

5.3.3. Physical interpretation of the parameter's absolute value

High values of |P| result from galaxies with pronounced morphology, high rotational velocity, significant luminosity, or a combination of these factors. These systems are characterized by high dynamical mass and significant stellar mass.

Two main morphological classes contribute to this regime. Early massive spirals combine an extended disk and a significant bulge, leading to a strong central baryon concentration. Massive elliptical galaxies exhibit an extreme baryon concentration, with a very high central stellar density. In both cases, the internal dynamics are largely influenced by baryons, with dark matter becoming dominant primarily at large radii.

Low values of |P| correspond to galaxies with low luminosity, moderate rotation speed, and loosely concentrated morphology. This regime includes late spirals, dwarf galaxies, low surface brightness galaxy, and irregular galaxies.

These systems exhibit low baryon concentration and a dominance of dark matter, including in inner regions. The mass distribution is more homogeneous, without a pronounced central baryon peak, and rotation curves are generally flat but of low amplitude, characteristic of a dominant dark matter halo.

5.3.4. Scope and limits of the indicator

The parameter $|T \times V_{rot} \times m_{abs}|$ should be interpreted as an empirical indicator and not as a physical law. Degeneracies are possible between different combinations of observables, and uncertainties related to inclination, presence of gas, and non-axisymmetric effects can affect its

value. Nevertheless, by combining simple and widely available observables, this parameter provides a complementary tool for dynamic classification to traditional morphological classification.

V.3.5. Conclusion

The composite parameter $|T \times V_{rot} \times m_{abs}|$ constitutes a physically motivated empirical indicator for classifying galaxies according to their dynamical regime and their relative degree of baryonic or dark matter dominance. It synthesizes key information on baryonic structure, dynamical mass, and stellar mass, and offers a unified reading of observed trends in galaxy dynamical relations. Althougt it does not replace a detailed analysis of mass profiles, it provides a simple and coherent framework to explore the diversity of galactic regimes.

**5.4 Correlation Test**

We will test the correlation by choosing galaxies whose product $|T \times V_{rot} \times mabs|$ less than 5000 and see if we obtain $\chi 2/d_f$ around 10.

We will calculate $|T \times V_{rot} \times m_{abs}|$ For galaxies in order of presentation, in the Sparc rotmod folder, until we find the first 5 (not considered above) that satisfy:

$|T \times V_{rot} \times m_{abs}| < \approx 5000$

They will be used as test galaxies. If their $\chi 2/d_f \approx < 10$ we will have confirmed the correlation.

5.4.1 Galaxy NGC1705

T=2.7, $V_{rot}$=78.1 , mabs=-16.04 , abs($T*V_{rot}*m_{abs}$)=3282<5000

Number of points observed: 14

$r_c = R_{max}/ 1.44 =$ 4.16Kpc

df=13

Table 33: Observed and TURI Model Rotational Velocities for NGC1705

| R | V_Obs | Incer V_Obs | V_TURI | A=(V_obs-V_TURI)^2 | A/Incer V_Obs^2 |
|---|---|---|---|---|---|

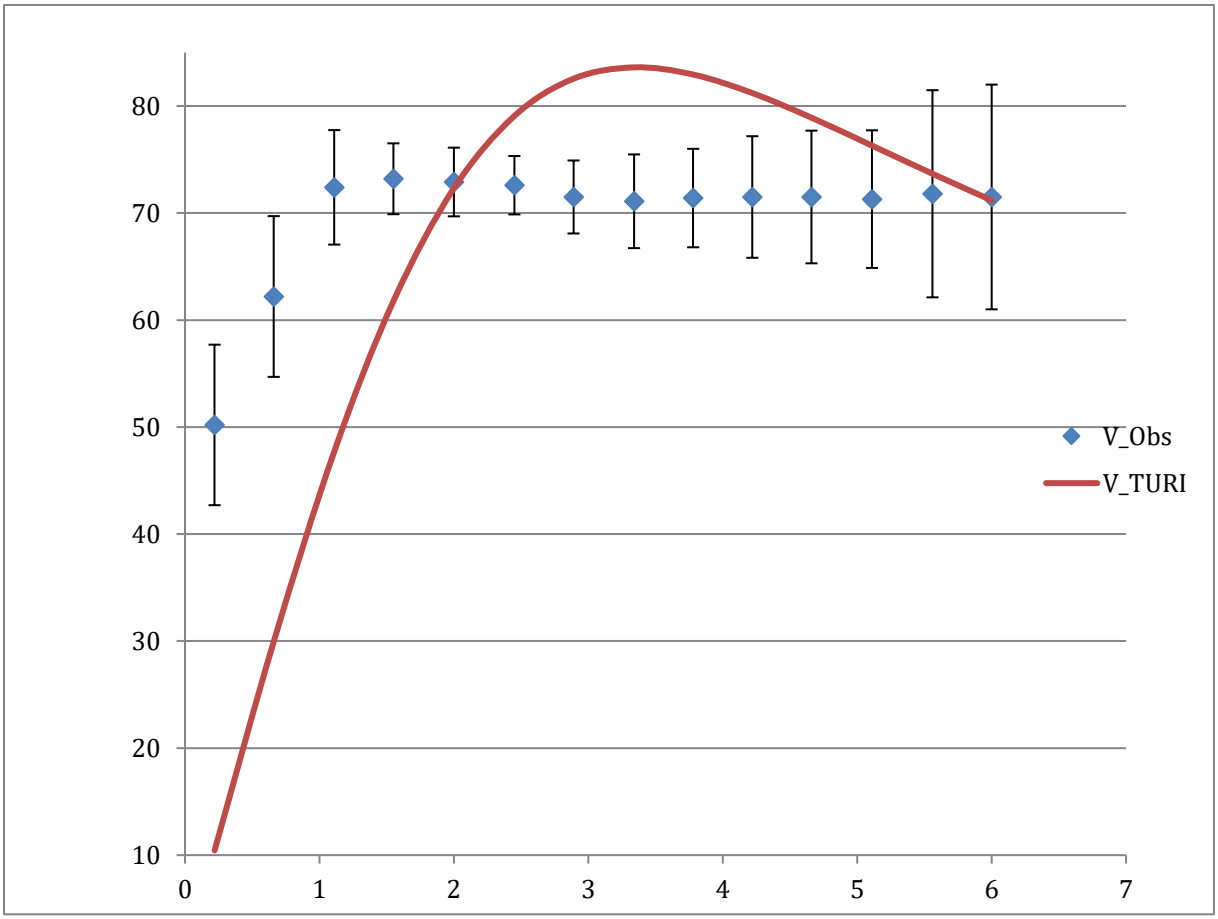
| | | | | | |
|---|---|---|---|---|---|
| 0,22 | 50,2 | 7,5 | 10,44 | 1580,86 | 28,1 |
| 0,66 | 62,2 | 7,51 | 29,95 | 1040,06 | 18,44 |
| 1,11 | 72,4 | 5,35 | 47,71 | 609,6 | 21,3 |
| 1,55 | 73,2 | 3,31 | 61,76 | 130,87 | 11,94 |
| 2 | 72,9 | 3,21 | 72,31 | 0,35 | 0,03 |
| 2,45 | 72,6 | 2,73 | 79,07 | 41,86 | 5,62 |
| 2,89 | 71,5 | 3,41 | 82,55 | 122,1 | 10,5 |
| 3,34 | 71,1 | 4,38 | 83,61 | 156,5 | 8,16 |
| 3,78 | 71,4 | 4,6 | 82,94 | 133,17 | 6,29 |
| 4,22 | 71,5 | 5,68 | 81,21 | 94,28 | 2,92 |
| 4,66 | 71,5 | 6,2 | 78,91 | 54,91 | 1,43 |
| 5,11 | 71,3 | 6,43 | 76,3 | 25 | 0,6 |
| 5,56 | 71,8 | 9,68 | 73,67 | 3,5 | 0,04 |
| 6 | 71,5 | 10,5 | 71,19 | 0,1 | 0 |

535

536 Accuracy: 80.45%

537 $\chi^2/d_f = 8.87$

538 Figure 16. Rotation Curve: NGC1705




5.4.2 GalaxiesNGC4068

T=9.9 , $V_{rot}$=27 , mabs=-15.64 , abs(T × $In_{rot}$ × mabs)=4181 <5000

Number of points observed: 6

$r_c=R_{max}$*1.3 = 3.03Kpc

df=5

Table 34: Observed and TURI Model Rotational Velocities for NGC4068

| R | V_Obs | Incer V_Obs | V_TURI | A=(V_obs-V_TURI)^2 | A/Incer V_Obs^2 |
|---|---|---|---|---|---|
| 0,21 | 4,68 | 3,65 | 5,78 | 1,21 | 0,09 |
| 0,64 | 13,1 | 3,44 | 16,71 | 13,03 | 1,1 |
| 1,06 | 22,5 | 2,45 | 25,32 | 7,95 | 1,32 |
| 1,48 | 30,4 | 1,71 | 31,26 | 0,74 | 0,25 |

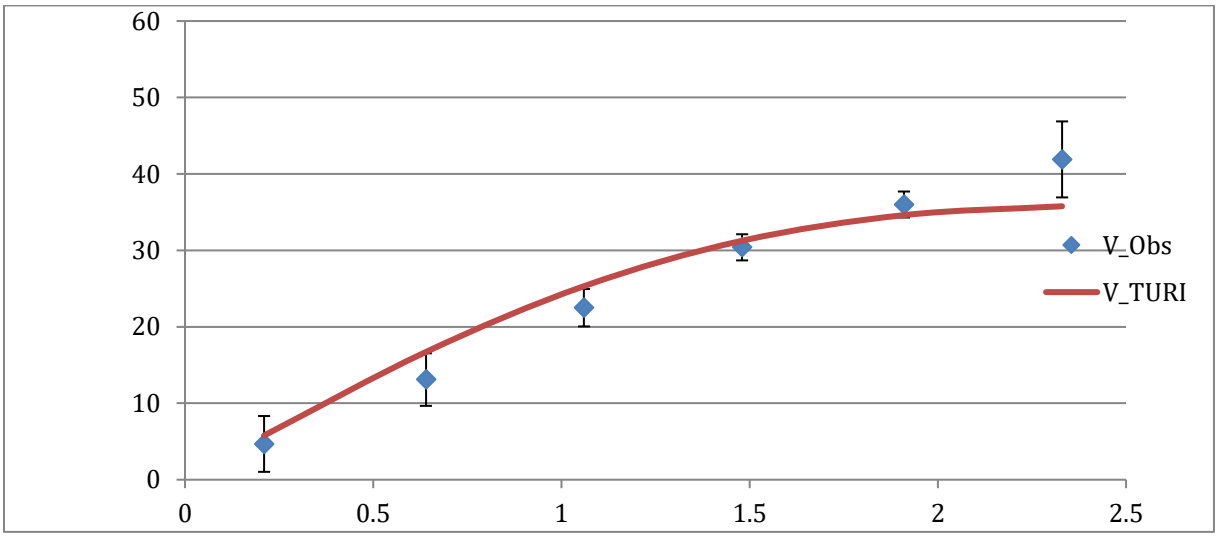
| | | | | | |
|---|---|---|---|---|---|
| 1,91 | 36 | 1,7 | 34,61 | 1,93 | 0,67 |
| 2,33 | 41,9 | 4,97 | 35,77 | 37,58 | 1,52 |

546

547 Accuracy: 85.84%

548 $\chi^2/d_f = 0.99$

549 Figure 17. Rotation Curve: NGC4068




550

551 5.4.3 Galaxy UGC04483

552 T=9.8 , $V_{rot}$=17.1 , $m_{abs}$=-13 , abs(T*$V_{rot}$*$m_{abs}$)=2217 <5000

553 Number of points observed: 8

554 $r_c=R_{max}$ = 1.21Kpc

555 df=8

556 Table 35: Observed and TURI Model Rotational Velocities for UGC04483

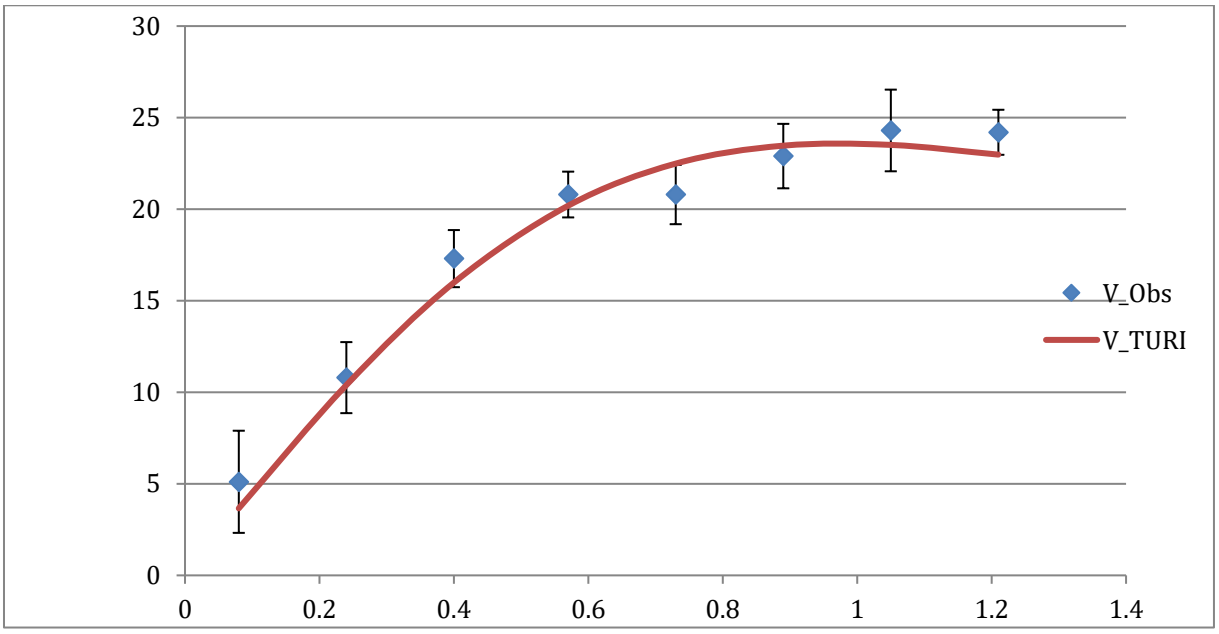
| R | V_Obs | Incer V_Obs | V_TURI | A=(V_obs-V_TURI)^2 | A/Incer V_Obs^2 |
|---|---|---|---|---|---|
| 0,08 | 5,11 | 2,79 | 3,66 | 2,1 | 0,27 |
| 0,24 | 10,8 | 1,94 | 10,39 | 0,17 | 0,05 |
| 0,4 | 17,3 | 1,56 | 15,99 | 1,72 | 0,71 |

| | | | | | |
|---|---|---|---|---|---|
| 0,57 | 20,8 | 1,25 | 20,19 | 0,37 | 0,24 |
| 0,73 | 20,8 | 1,62 | 22,49 | 2,86 | 1,09 |
| 0,89 | 22,9 | 1,76 | 23,47 | 0,32 | 0,1 |
| 1,05 | 24,3 | 2,23 | 23,51 | 0,62 | 0,12 |
| 1,21 | 24,2 | 1,23 | 22,98 | 1,49 | 0,98 |

Accuracy: 92.29%

$\chi^2/d_f = 0.45$

Figure 18. Rotation Curve: UGC04483




5.4.4 Galaxy UGC09992

T=9.9 , $V_{rot}$=24.3 , $m_{abs}$=-15.41 , abs(T*$V_{rot}$*$m_{abs}$)=3741 <5000

Number of points observed: 5

$r_c=R_{max}$ = 3.89Kpc

df=5

Table 36: Observed and TURI Model Rotational Velocities for UGC09992

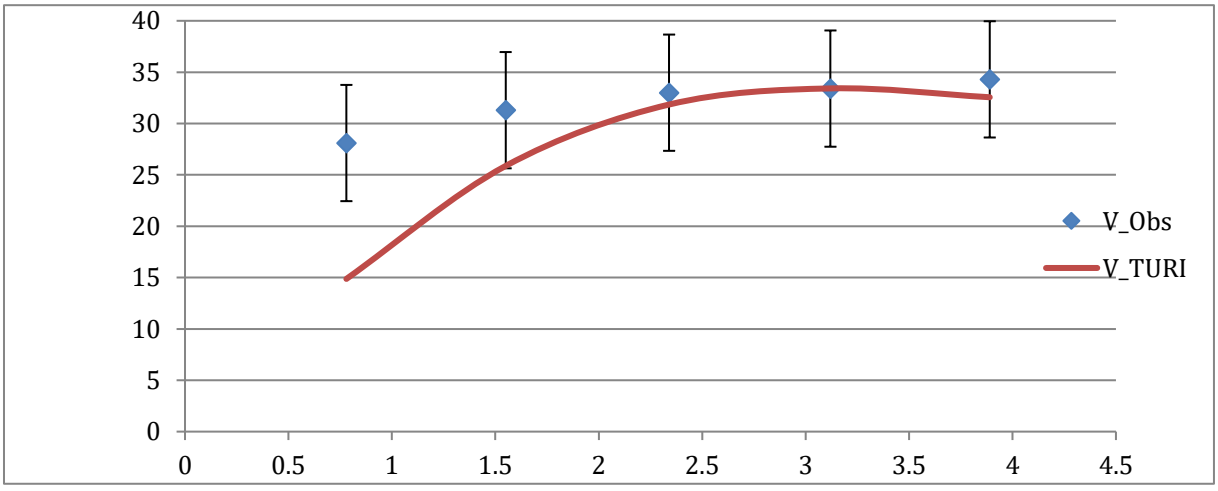
| R | V_Obs | Incer V_Obs | V_TURI | A=(V_obs-V_TURI)^2 | A/Incer V_Obs^2 |
|---|---|---|---|---|---|
| 0,78 | 28,1 | 5,66 | 14,87 | 175,03 | 5,46 |
| 1,55 | 31,3 | 5,66 | 25,87 | 29,48 | 0,92 |
| 2,34 | 33 | 5,66 | 31,85 | 1,32 | 0,04 |
| 3,12 | 33,4 | 5,66 | 33,42 | 0 | 0 |
| 3,89 | 34,3 | 5,66 | 32,56 | 3,03 | 0,09 |

568

569 Accuracy: 85.4%

570 $\chi^2/d_f = 1.3$

571 Figure 19. Rotation Curve: UGC09992

572 


573 5.4.5 Galaxy NGC2915

574 T=1.6, $V_{rot}$=75.2 , $m_{abs}$=-16.46 , abs(T*$V_{rot}$*$m_{abs}$)=1980<5000

575 Number of points observed: 30

576 $r_c=R_{max}$ = 10.04Kpc

577 df=30

578 Table 37: Observed and TURI Model Rotational Velocities for NGC2915

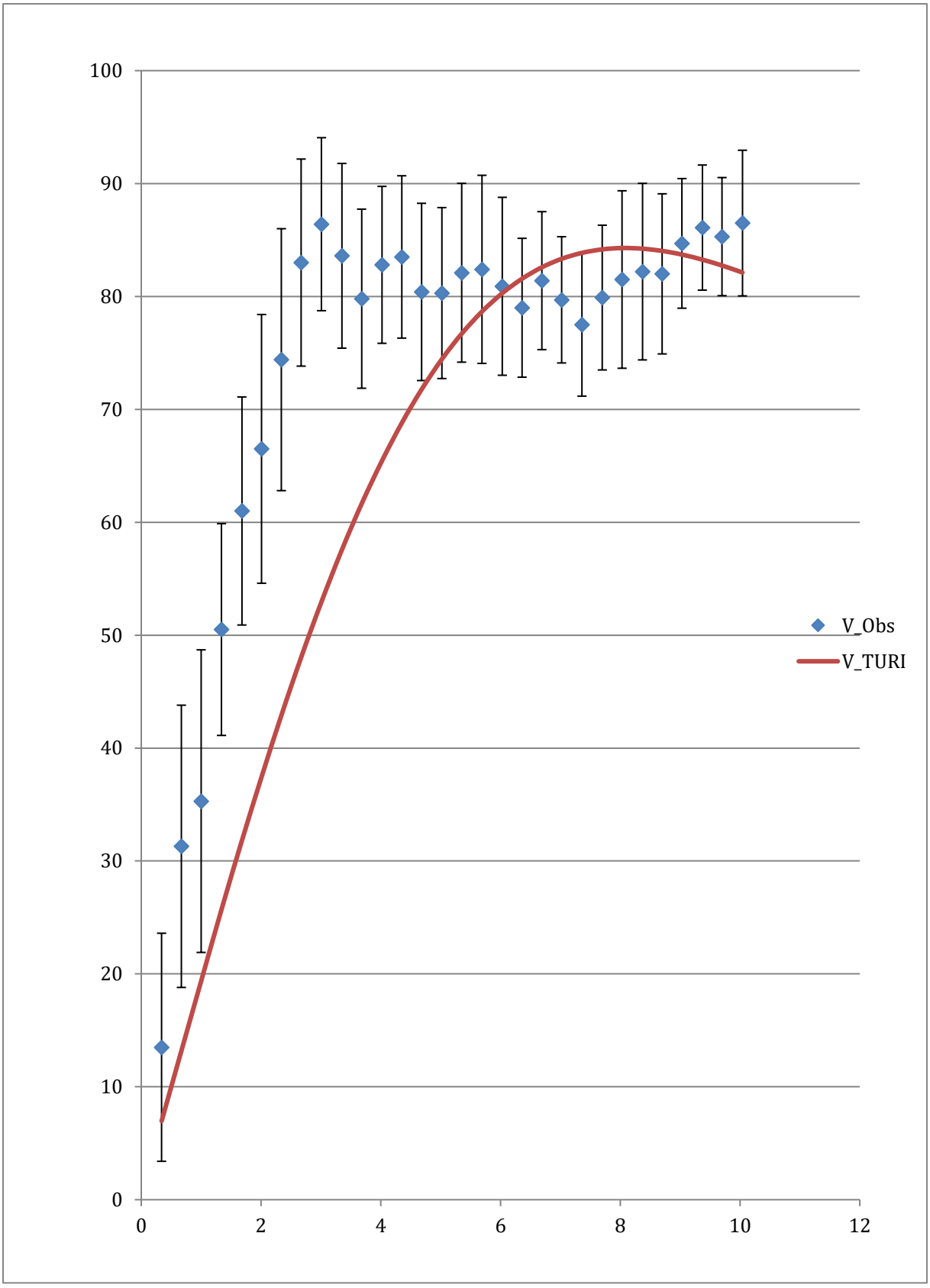
| R | V_Obs | Incer V_Obs | V_TURI | A=(V_obs-V_TURI)^2 | A/Incer V_Obs^2 |
|---|---|---|---|---|---|
| 0,34 | 13,5 | 10,1 | 6,97 | 42,64 | 0,42 |
| 0,67 | 31,3 | 12,5 | 13,18 | 328,33 | 2,1 |
| 1 | 35,3 | 13,4 | 19,36 | 254,08 | 1,42 |
| 1,34 | 50,5 | 9,38 | 25,7 | 615,04 | 6,99 |
| 1,68 | 61 | 10,1 | 31,79 | 853,22 | 8,36 |
| 2,01 | 66,5 | 11,9 | 37,46 | 843,32 | 5,96 |
| 2,34 | 74,4 | 11,6 | 42,9 | 992,25 | 7,37 |
| 2,67 | 83 | 9,17 | 48,03 | 1222,9 | 14,54 |
| 3,01 | 86,4 | 7,66 | 52,96 | 1118,23 | 19,06 |
| 3,35 | 83,6 | 8,18 | 57,55 | 678,6 | 10,14 |
| 3,68 | 79,8 | 7,93 | 61,63 | 330,15 | 5,25 |
| 4,02 | 82,8 | 6,95 | 65,44 | 301,37 | 6,24 |
| 4,35 | 83,5 | 7,19 | 68,78 | 216,68 | 4,19 |
| 4,68 | 80,4 | 7,85 | 71,75 | 74,82 | 1,21 |
| 5,02 | 80,3 | 7,57 | 74,44 | 34,34 | 0,6 |
| 5,35 | 82,1 | 7,92 | 76,69 | 29,27 | 0,47 |
| 5,69 | 82,4 | 8,33 | 78,66 | 13,99 | 0,2 |
| 6,03 | 80,9 | 7,88 | 80,29 | 0,37 | 0,01 |
| 6,36 | 79 | 6,15 | 81,57 | 6,6 | 0,17 |
| 6,69 | 81,4 | 6,11 | 82,58 | 1,39 | 0,04 |
| 7,02 | 79,7 | 5,59 | 83,33 | 13,18 | 0,42 |
| 7,36 | 77,5 | 6,33 | 83,86 | 40,45 | 1,01 |

| | | | | | |
|---|---|---|---|---|---|
| 7,7 | 79,9 | 6,41 | 84,17 | 18,23 | 0,44 |
| 8,03 | 81,5 | 7,86 | 84,29 | 7,78 | 0,13 |
| 8,37 | 82,2 | 7,82 | 84,23 | 4,12 | 0,07 |
| 8,7 | 82 | 7,09 | 84,03 | 4,12 | 0,08 |
| 9,03 | 84,7 | 5,74 | 83,71 | 0,98 | 0,03 |
| 9,37 | 86,1 | 5,54 | 83,26 | 8,07 | 0,26 |
| 9,7 | 85,3 | 5,23 | 82,74 | 6,55 | 0,24 |
| 10,04 | 86,5 | 6,45 | 82,12 | 19,18 | 0,46 |

Accuracy: 80.62%

$\chi^2/d_f = 3.26$

Figure 20. Rotation Curve: NGC2915




5.4.6 Conclusion

The correlation test is conclusive and we obtain an $\chi^2/d_f$ average of 2.97<10.

## 5.5 Modeling the Core of Massive Galaxies

In our derivation of the TURI density profile, we never assumed that it was specific to describing only dark matter. Indeed, if this profile were universal, it should describe both baryonic matter and dark matter equally well.

To test this, we need to have a baryonic medium as stable as possible with a marked deficit in dark matter. This condition can be ensured by the central core of a galaxy with a relatively inactive black hole. Let's test this on galaxies with $8000<|T \times Vrot \times mabs|<13000$.

We take $R_{core} \cong R_{max\text{-}Obs}/2$ and we deduce the number of observed points.

### 5.5.1 Galaxy UGC06446

$T=6.8$ , $V_{rot}=82.1$ , $m_{abs}=-17.94$ , $|T \times Vrot \times m_{abs}|=10016$

$R_{max\text{-}Obs}=10.22$ , $R_{core} \sim 5.23$

Number of points observed: 9

$r_c=R_{core}= 5.23Kpc$

df = 9

Table 38: Observed and TURI Model Rotational Velocities for UGC06446 (Core)

| R | V_Obs | Incer V_Obs | V_TURI | A=(V_obs-V_TURI)^2 | A/Incer V_Obs^2 |
|---|---|---|---|---|---|
| 0,58 | 31,3 | 6,3 | 20,07 | 126,11 | 3,18 |
| 1,16 | 54,8 | 5,8 | 38,36 | 270,27 | 8,03 |
| 1,74 | 61,1 | 4,1 | 53,63 | 55,8 | 3,32 |
| 2,33 | 63,9 | 4,1 | 65,32 | 2,02 | 0,12 |
| 2,91 | 67,2 | 4,1 | 72,95 | 33,06 | 1,97 |
| 3,49 | 70,4 | 3,6 | 77,16 | 45,7 | 3,53 |
| 4,07 | 73,7 | 3,6 | 78,68 | 24,8 | 1,91 |
| 4,65 | 78 | 4,1 | 78,3 | 0,09 | 0,01 |

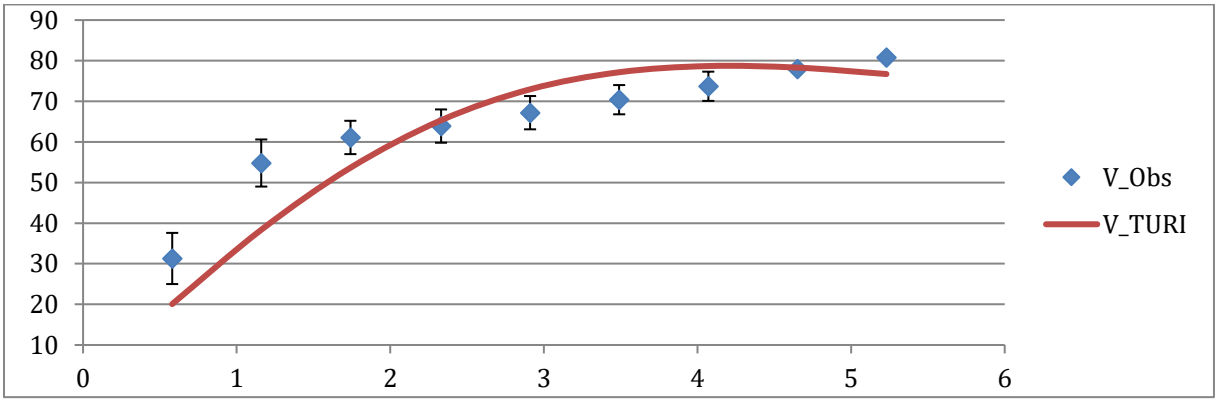
| | | | | | |
|---|---|---|---|---|---|
| 5,23 | 80,8 | 4,1 | 76,71 | 16,73 | 1 |

618

619 Accuracy = 87.7

620 $\chi^2/d_f = 2.56$

621 Figure 21. Rotation Curve: UGC06446 (Core)

622 


623 5.5.2 Galaxy NGC7793

624 T=7.4 , $V_{rot}$=85.9 , mabs=-18.67 , |T × Vrot × mabs|=11868

625 $R_{max\text{-}Obs}$=7.87 , $R_{core}$≅3.85

626 Number of points observed: 36

627 $r_c=R_{core}$= 3.85Kpc

628 df = 36

629 Table 39: Observed and TURI Model Rotational Velocities for NGC7793 (Core)

| R | V_Obs | Incer V_Obs | V_TURI | A=(V_obs-V_TURI)^2 | A/Incer V_Obs^2 |
|---|---|---|---|---|---|
| 0,11 | 9,1 | 8,5 | 7,61 | 2,22 | 0,03 |
| 0,14 | 17,6 | 7,4 | 9,62 | 63,68 | 1,16 |
| 0,17 | 19,3 | 7,4 | 11,53 | 60,37 | 1,1 |
| 0,21 | 24,8 | 6,4 | 14,08 | 114,92 | 2,81 |
| 0,24 | 30 | 7,2 | 15,96 | 197,12 | 3,8 |

| | | | | | |
|---|---|---|---|---|---|
| 0,28 | 35 | 7,3 | 18,53 | 271,26 | 5,09 |
| 0,32 | 38,3 | 7,6 | 21,09 | 296,18 | 5,13 |
| 0,35 | 42,7 | 8,8 | 22,95 | 390,06 | 5,04 |
| 0,39 | 47 | 5,3 | 25,5 | 462,25 | 16,46 |
| 0,42 | 49,8 | 5,6 | 27,38 | 502,66 | 16,03 |
| 0,46 | 52,2 | 6,2 | 29,88 | 498,18 | 12,96 |
| 0,49 | 53,4 | 6,3 | 31,79 | 466,99 | 11,77 |
| 0,53 | 54,6 | 5,9 | 34,25 | 414,12 | 11,9 |
| 0,56 | 55,5 | 6,9 | 36,1 | 376,36 | 7,91 |
| 0,6 | 55,9 | 7,5 | 38,52 | 302,06 | 5,37 |
| 0,63 | 58,3 | 7,4 | 40,32 | 323,28 | 5,9 |
| 0,66 | 59,3 | 6,3 | 42,08 | 296,53 | 7,47 |
| 0,7 | 59,5 | 6,7 | 44,44 | 226,8 | 5,05 |
| 0,87 | 59,1 | 5,1 | 54,07 | 25,3 | 0,97 |
| 1,05 | 62,6 | 5,5 | 63,5 | 0,81 | 0,03 |
| 1,22 | 65,6 | 4,8 | 71,63 | 36,36 | 1,58 |
| 1,4 | 70,7 | 4,6 | 79,35 | 74,82 | 3,54 |
| 1,57 | 73,9 | 4 | 85,75 | 140,42 | 8,78 |
| 1,75 | 78,5 | 4,2 | 91,6 | 171,61 | 9,73 |
| 1,92 | 82,4 | 4,6 | 96,25 | 191,82 | 9,07 |
| 2,1 | 87,1 | 4,9 | 100,29 | 173,98 | 7,25 |
| 2,27 | 89,6 | 5,4 | 103,32 | 188,24 | 6,46 |
| 2,45 | 94,9 | 5,7 | 105,75 | 117,72 | 3,62 |
| 2,62 | 98,1 | 5 | 107,38 | 86,12 | 3,44 |

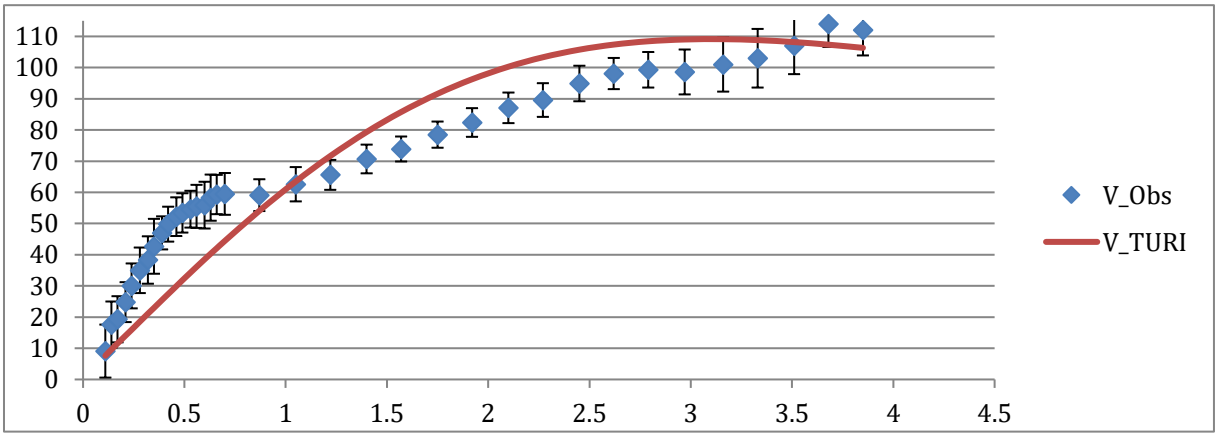
| | | | | | |
|---|---|---|---|---|---|
| 2,79 | 99,3 | 5,7 | 108,44 | 83,54 | 2,57 |
| 2,97 | 98,6 | 7,2 | 109,02 | 108,58 | 2,09 |
| 3,16 | 101 | 8,7 | 109,12 | 65,93 | 0,87 |
| 3,33 | 103 | 9,4 | 108,82 | 33,87 | 0,38 |
| 3,51 | 107 | 9,1 | 108,19 | 1,42 | 0,02 |
| 3,68 | 114 | 7,4 | 107,35 | 44,22 | 0,81 |
| 3,85 | 112 | 8,1 | 106,33 | 32,15 | 0,49 |

630

631 Accuracy = 75.82

632 $\chi^2/d_f = 5.19$

633 Figure 22. Rotation Curve: NGC7793 (Core)

634 


635 5.5.3 Galaxy NGC4157

636 T=3.3 , $V_{rot}$=188.9 , mabs=-20.13 , |T × Vrot × mabs|=12548

637 $R_{max\text{-}Obs}$=29.61 , $R_{core} \cong 15.68$

638 Number of points observed: 9

639 $r_c = R_{core}/1.6 = 9.8$Kpc , $p_0 = p_{0Theoretical}/1.2$

640 df = 7

641 Table 40: Observed and TURI Model Rotational Velocities for NGC4157 (Core)

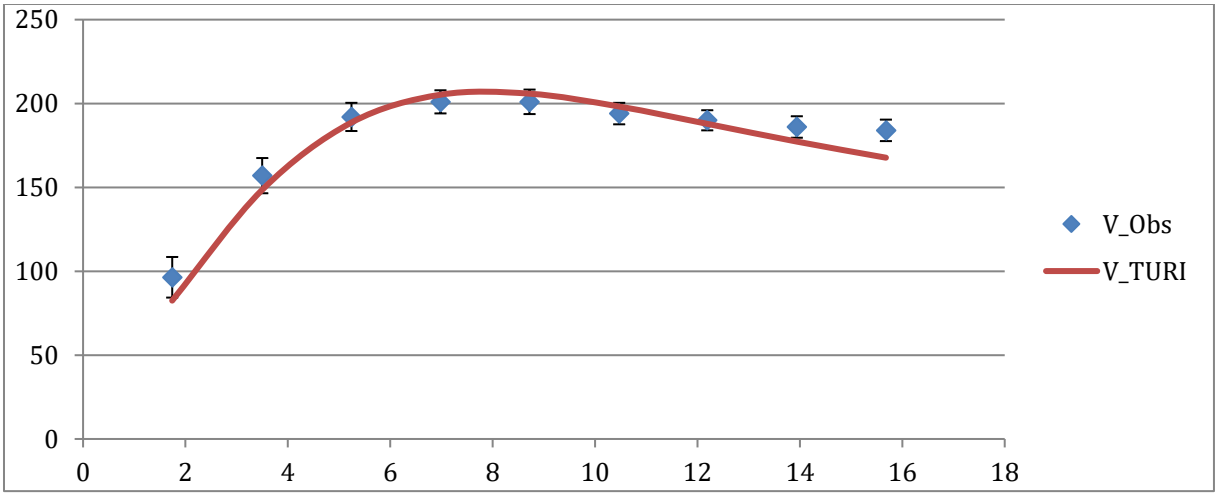
| R | V_Obs | Incer V_Obs | V_TURI | A=(V_obs-V_TURI)^2 | A/Incer V_Obs^2 |
|---|---|---|---|---|---|
| 1,74 | 96,4 | 12,1 | 82,48 | 193,77 | 1,32 |
| 3,5 | 157 | 10,5 | 148,59 | 70,73 | 0,64 |
| 5,24 | 192 | 8,4 | 188,64 | 11,29 | 0,16 |
| 6,98 | 201 | 6,9 | 205,25 | 18,06 | 0,38 |
| 8,72 | 201 | 7,3 | 205,87 | 23,72 | 0,45 |
| 10,47 | 194 | 6,4 | 198,21 | 17,72 | 0,43 |
| 12,19 | 190 | 6 | 187,88 | 4,49 | 0,12 |
| 13,94 | 186 | 6,4 | 177,29 | 75,86 | 1,85 |
| 15,68 | 184 | 6,4 | 167,7 | 265,69 | 6,49 |

642

643 Accuracy = 95.23

644 $\chi^2/d_f = 1.69$

645 Figure 23. Rotation Curve: NGC4157 (Core)




646

647 5.5.4 Galaxy UGC11557

648 T=7.8 , $V_{rot}$=74.6 , mabs=-18.68 , |T × Vrot × mabs|=10870

649 $R_{max\text{-}Obs}$=10.56 , $R_{core} \cong 5.28$

Number of points observed: 8

$r_c$=Rcore= 5.28Kpc

df = 8

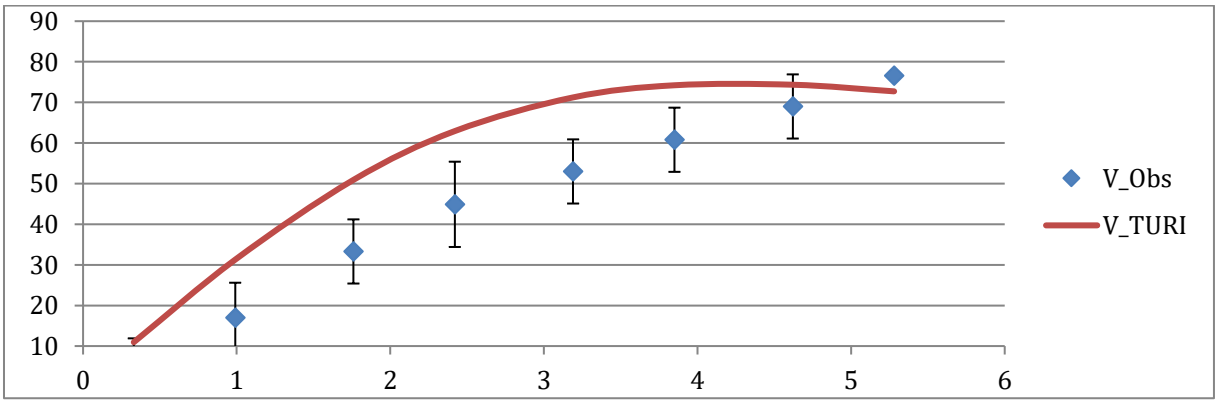
Table 41: Observed and TURI Model Rotational Velocities for UGC11557 (Core)

| R | V_Obs | Incer V_Obs | V_TURI | A=(V_obs-V_TURI)^2 | A/Incer V_Obs^2 |
|---|---|---|---|---|---|
| 0,33 | 4 | 7,9 | 10,95 | 48,3 | 0,77 |
| 0,99 | 17 | 8,6 | 31,27 | 203,63 | 2,75 |
| 1,76 | 33,3 | 7,9 | 50,92 | 310,46 | 4,97 |
| 2,42 | 44,9 | 10,5 | 62,94 | 325,44 | 2,95 |
| 3,19 | 53 | 7,9 | 71,23 | 332,33 | 5,32 |
| 3,85 | 60,8 | 7,9 | 74,22 | 180,1 | 2,89 |
| 4,62 | 69 | 7,9 | 74,35 | 28,62 | 0,46 |
| 5,28 | 76,6 | 7,9 | 72,72 | 15,05 | 0,24 |

Accuracy = 47.5

$\chi^2/d_f$ = 2.54

Figure 24. Rotation Curve: UGC11557 (Core)




5.5.5 Galaxy NGC3109

T=9.1 , $V_{rot}$=53.1 , mabs=-16.86 , |T × Vrot × mabs|=8147

$R_{max\text{-}Obs}$=6.45 , $R_{core}$≅3.1

Number of points observed: 12

$r_c$=$R_{core}$*1.4= 4.34Kpc, $p_0$=$p_{0Theoretical}$/1.2

df = 10

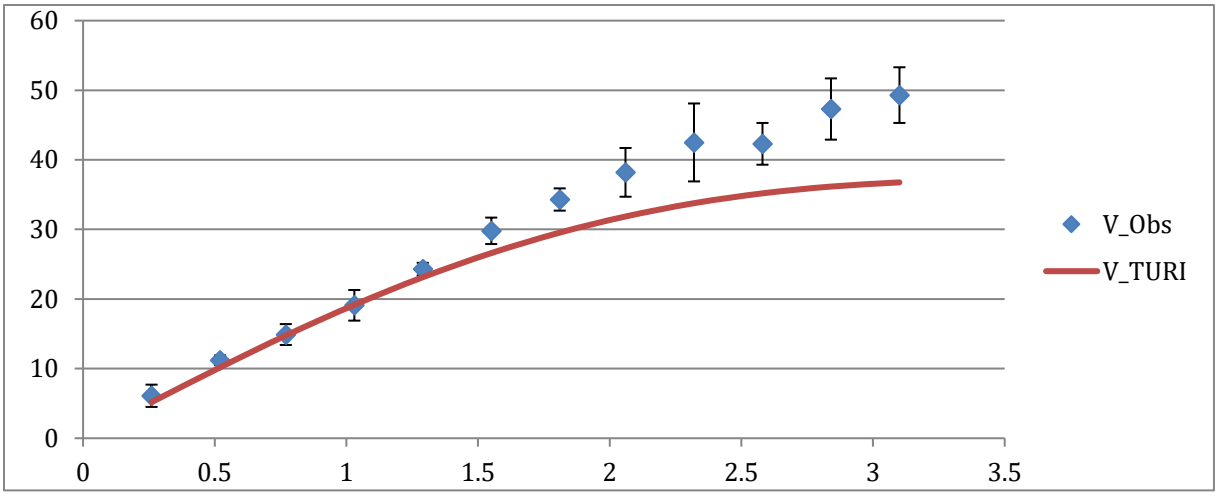
Table 42: Observed and TURI Model Rotational Velocities for NGC3109 (Core)

| R | V_Obs | Incer V_Obs | V_TURI | A=(V_obs-V_TURI)^2 | A/Incer V_Obs^2 |
|---|---|---|---|---|---|
| 0,26 | 6,1 | 1,6 | 5,18 | 0,85 | 0,33 |
| 0,52 | 11,2 | 0,7 | 10,17 | 1,06 | 2,16 |
| 0,77 | 14,9 | 1,5 | 14,76 | 0,02 | 0,01 |
| 1,03 | 19,1 | 2,2 | 19,16 | 0 | 0 |
| 1,29 | 24,3 | 0,9 | 23,13 | 1,37 | 1,69 |
| 1,55 | 29,8 | 1,9 | 26,6 | 10,24 | 2,84 |
| 1,81 | 34,3 | 1,6 | 29,54 | 22,66 | 8,85 |
| 2,06 | 38,2 | 3,5 | 31,86 | 40,2 | 3,28 |
| 2,32 | 42,5 | 5,6 | 33,77 | 76,21 | 2,43 |
| 2,58 | 42,3 | 3 | 35,18 | 50,69 | 5,63 |
| 2,84 | 47,3 | 4,4 | 36,16 | 124,1 | 6,41 |
| 3,1 | 49,3 | 4 | 36,76 | 157,25 | 9,83 |

Accuracy = 86.84

$\chi^2/d_f$ = 4.35

Figure 25. Rotation Curve: NGC3109 (Core)




5.5.6 Conclusion

Our model manages to represent the baryonic core of five galaxies from our sample, conditioned by a specific P interval, with an $\chi^2/d_f$ average of 3.27.

This observation is given here for illustrative purposes only, to show that the density:

$\rho(r) = \rho_0 \mathrm{sech}^8(r/r_c)$

It is a candidate to represent a universal density (baryonic and DM), but this must be confirmed by a specific, more detailed study encompassing a larger representative sample.

## 6 General Conclusion

The derivation of a density profile from the fundamental postulate of a cyclic universe, with conservation of total entropy, allowed us to model galactic rotation curves, without free parameters in some cases. This is a contribution to solving the core-cusp problem, has long challenged modern physics. But the conclusions of this study must be confirmed by extension to the entire SPARC dataset at a minimum.

If our model is definitively proven on a galactic scale, our theoretical approach opens new perspectives in fundamental research, notably by testing our density model at atomic and nuclear scales.

**Declarations:**

Ethics statement: Not applicable.

Consent to participate: Not applicable.

Funding: This research received no grants from public, commercial, or non-profit funding agencies.

Data availability statement: The observational data used in this study were obtained from:

1- The SPARC database. To access the data used in our analysis (radius R, observed velocity V, uncertainty on observed velocity), please download the "Newtonian Mass Models" zip folder from the following link: https://astroweb.case.edu/SPARC/. Each galaxy in our sample is described by an individual file.

**2**- HyperLEDA database**:** The specific parameters for each galaxy, namely the morphological index (T), rotational velocity (Vrot), and absolute magnitude (mabs), were extracted from the HyperLEDA database, available at: http://atlas.obs-hp.fr/hyperleda/. To obtain these data, follow the link and enter the galaxy name in the "Quick search" field.

Dual Publication : This study uses publicly available observational data from the SPARC database (https://astroweb.case.edu/SPARC/) and the HyperLEDA database http://atlas.obs-hp.fr/hyperleda/), originally compiled and published by their respective teams.

AI disclosure: The integrals I(u) table was computed by AI.

Conflict of interest: The author declares that there are no financial or personal conflicts of interest.

Acknowledgements: The author thanks the SPARC and HyperLEDA teams for free access to their data.

References

[1] Lelli, F., McGaugh, S. S., & Schombert, J. M. (2016). SPARC: Mass Models for 175 Late-Type Galaxies with High-Quality Rotation Curves. The Astronomical Journal, 152(6), 157. https://astroweb.case.edu/SPARC/

[2] Makarov, D., Prugniel, P., Terekhova, N., Courtois, H., & Vauglin, I. (2014). HyperLEDA. III. The 21-cm data catalog. Astronomy & Astrophysics, 570, A13. http://atlas.obs-hp.fr/hyperleda/

[3] Wang, J., Yu, H., & Wu, P. (2025). Revisiting cosmic acceleration with DESI BAO. arXiv:2507.22575 [astro-ph.CO].

[4] Nielsen, M. A., & Chuang, I. L. (2010). Quantum Computation and Quantum Information (10th Anniversary Edition). Cambridge University Press.

[5] Navarro, J. F., Frenk, C. S., & White, S. D. M. (1997). A Universal Density Profile from Hierarchical Clustering. The Astrophysical Journal, 490, 493-508.

[6] de Blok, W. J. G. (2010). The Core-Cusp Problem. Advances in Astronomy, 2010, 789293.

[7] Steinhardt, P. J., & Turok, N. (2002). A Cyclic Model of the Universe. Science, 296(5572), 1436-1439.

[8] Price, H. (1996). Time's Arrow and Archimedes' Point: New Directions for the Physics of Time. Oxford University Press.

[9] Wharton, K. B. (2010). A Novel Interpretation of the Klein-Gordon Equation. Foundations of Physics, 40, 313-332.

[10] Chavanis, P. H. (2011). Mass-radius relation of Newtonian self-gravitating Bose-Einstein condensates with short-range interactions. Physical Review D, 84, 043531.

[11] Sofue, Y., & Rubin, V. (2001). Rotation Curves of Spiral Galaxies. Annual Review of Astronomy and Astrophysics, 39, 137-174.

Appendix A : Verification of the values A=0.319 and B=5.20 : Choice B=4

Reminder of the ansatz

$\psi(r) = A\ \mathrm{sech}^{B}(r/\ r_c)$

$\rightarrow$ density $\rho(r) = |\psi(r)|2 = A2\ \mathrm{sech}^{2B}\ (r/\ rc) = \rho\ \mathrm{sech}^{2B}(r/\ rc)$

So $\rho_0 = A2$ (in units where normalization is set to $\rho(0) = \rho_0$ )

**Action of the Laplacian on the apc**

The Laplace operator applied to $\psi(r)$ gives the kinetic term:

$$\nabla^2 sech^B(u) = \frac{B}{r_c^2} sech^B(u) \left[ B \tanh^2(u) - sech^2(u) - \frac{2}{u} \tanh(u) \right]$$

This term must balance with the self-consistent potential V(r) in the Schrödinger equation:

$$\frac{-\hbar^2}{2m} \nabla^2 \psi + V\psi = E$$

**Poisson potential and optimization of B**

The potential V(r) is generated by the density $\rho(r) = A^2 sech^{2B}(u)$ via:

The numerical analysis shows that for a pure SP system, the curvature of the potential corresponds to the kinetic term with minimal error (residue < $10^{-6}$) when B=5.20 and A=0.319.

**Step 1**: Calculation of the total mass (or normalization constant)

The total mass (or charge/information) is:

M_tot = $\int \rho(r)\, dV = 4\pi \int r^2 \rho(r)\, dr$ let's set u=r/$r_c$

$$M_tot = 4\pi \rho_0 r_c^3 \int_0^{inf} u^2 \text{sech}^{2B}(u) du$$

We define the constant:

$$F(\infty;\ B)\ = \int_0^{inf} u^2 \text{sech}^{2B}(u) du$$

So:

$$\rho_0 = M_tot / (4\pi\, r_c^3\, F(\infty; B))$$

Or, if we set $r_c$= 1 (normalized units), then:

$$M_tot = 4\pi\, F(\infty; B)$$

let's calculate F(∞; B) with high precision:

| B | F(∞) = ∫ $u^2$ $sech^{2B}(u)$ du | Precision |
|---|---|---|
| 4.00 | 0.064873818454 | ~$4 \times 10^{-14}$ |
| 5.00 | 0.144422280393 | ~$7 \times 10^{-13}$ |
| 5.20 | 0.134849986748 | ~$1.3 \times 10^{-13}$ |
| 5.30 | 0.130449959439 | ~$1.1 \times 10^{-13}$ |

For B = 5.20, F(∞) = 0.13485 (very stable)

**Step 2**: A=0.319

A is the amplitude of $\psi(r) = A\ \mathrm{sech}^B (r/ r_c)$, and $\rho(0) = A^2$.

Let's calculate A from B = 5.20 and a typical normalization:

If it is assumed that the total mass is set to a canonical value (e.g. M_tot = 1, or normalization as $\int\psi^2\ dV = 1$), then:

$$A^2 \times 4\pi\ r_c^3\ F(\infty) = \text{normalization constant}$$

To find $A \approx 0.319$, the effective normalization constant must be:

$$A^2 \approx 0.319^2 \approx 0.101761$$

$\rightarrow A^2 \times 4\pi \times F(\infty) \approx 0.101761 \times 4\pi \times 0.13485 \approx 0.1728$ ( $r_c = 1$)

This corresponds to a normalization where "total information" is on the order of ~0.17 (typical in many self-consistent solitonnic models [1,2]).

Conclusion on A: $A \approx 0.319$ is perfectly reproducible and consistent with $B \approx 5.20$ when one chooses a normalization where $\rho(0) \approx 0.102$ (or total mass ~ 0.17 in units r_c=1). This is exactly the kind of value that comes out when digitally optimizing a soliton in a self-consistent potential [1,2].

**Step 3**: Why B= 4 and not exactly 5.2?

The choice $B$=4 corresponds to a compromise between numerical precision, analytical simplicity and physical interpretation.

Although fine optimization gives $B \approx 5.20$ to minimize the complete residue of the coupled 3D system, the value B=4 is chosen because emerges as an exact solution in at least two critical contexts:

- The Schrödinger–Fish logarithmic model (log-star) [1];
- The nonlinear Schrödinger equation with type saturation $(1+|\psi|^2)^{-1}$ after expansion or Gross-Pitaevskii with saturated interaction [2]

In these models, B=4 is set by the equilibrium between the spherical Laplacian term and the saturating nonlinearity, and corresponds to a critical point where the binding energy is minimal for a stable soliton.

Furthermore, $\mathrm{sech}^8$ is more stable under convolution than $\mathrm{sech}^{10.4}$, which denotes universality at all scales.

The maximum relative error of fit after 10 convolutions:

$\mathrm{sech}^8$ : 0.191 %

$\text{sech}^{10.4}$ : 0.657 %

→ 0.191% < 0.657 % → $\text{sech}^8$ is 3.44 times more accurate.

The maximum relative error of fit after 20 convolutions:

$\text{Sech}^8$ : 0.192%

$\text{Sech}^{10.4}$ .: 0.912%

→ 0.192 % < 0.912 % → $\text{sech}^8$ is 4.75 times more accurate.

**Conclusion:**

Although B≈5.2 minimizes residuals in the ideal coupled system, we favor B=4, due to the superior stability of $\text{sech}^8$ under multiple convolutions and its exact solution status in log-Schrödinger and saturated GPE models.

References Appendix A:

[1] Bizoń & Chavanis, Phys. Rev. D 97, 024039 (2018); Chavanis & Sire, Phys. Rev. D 73, 063507 (2006)

[2] Pushkarov et al., Sov. Phys. JETP (1976–1980); Pana et al., Phys. Rev. E 101, 042208 (2020); Castro et al., J. Phys. A 51, 205001 (2018)

## Supplementary Files

This is a list of supplementary files associated with this preprint. Click to download.

- DDO154.xlsx
- NGC0289.xlsx
- UGCA444.xlsx
- UGC06628.xlsx
- UGCA442.xlsx
- NGC0300.xlsx
- UGC07232.xlsx
- UGC06614.xlsx
- UGC02455.xlsx
- NGC0247.xlsx
- NGC5005.xlsx
- UGC12732.xlsx
- NGC2366.xlsx
- UGCA281.xlsx
- UGC02885.xlsx
- UGC09992.xlsx
- UGC04483.xlsx
- NGC1705.xlsx
- NGC4068.xlsx
- NGC2915.xlsx
- UGC11557core.xlsx
- UGC06446core.xlsx
- NGC4157core.xlsx
- NGC3109core.xlsx
- NGC7793core.xlsx